IEEE Geoscience and Remote Sensing Magazine, Available online 24 March 2025
DOI: 10.1109/mgrs.2025.3535412

Distributed Spaceborne SAR: A Review of Systems, Applications, and Road Ahead

Cheng Hu, *Senior Member, IEEE*, Yuanhao Li, *Member, IEEE*, Zhiyang Chen, *Member, IEEE*, Feifeng Liu, Qingjun Zhang, Andrea Monti-Guarnieri, *Senior Member, IEEE,* Stephen Hobbs, Andrei Anghel, *Senior Member, IEEE*, Mihai Datcu, *Fellow, IEEE*

***Abstract*—As a crucial sensor for wide-area Earth observation, Spaceborne Synthetic Aperture Radar (SAR) plays a pivotal role in large-scale terrain mapping, ocean observation, disaster monitoring, etc. Driven by the increasing demands for diverse applications, enhanced performance, and the continuous advancement of satellite and radar technologies, the distributed configuration has emerged as a key developmental trend for spaceborne SAR. This review comprehensively summarizes the systems and typical applications of distributed spaceborne SAR. The system configurations encompass homogenous distributed SAR, formed by multiple identical or similar platforms, and heterogeneous distributed SAR, characterized by significant differences between the transmitting and receiving platforms. Typical applications of distributed SAR include intelligent target recognition, terrain mapping, deformation retrieval, atmosphere measurement, ocean observation, among others. Finally, the review offers a prospective outlook on the future development of distributed spaceborne SAR.**

I. INTRODUCTION

Spaceborne Synthetic Aperture Radar (SAR) utilizes radar payloads mounted on satellite platforms to emit wideband signals in the range direction and leverages synthetic aperture in the azimuth direction to achieve two-dimensional imaging over a large area [1]. The first spaceborne SAR, SeaSat, was launched by the United States (U.S.) in 1978 [2]. Nowadays, more countries and organizations including the European Space Agency (ESA), Canada, Japan, and China have successfully developed spaceborne SARs [3, 4]. These spaceborne SAR systems have avoided the limitations of point-by-point measurements of traditional ground-based sensors, thus have now become an indispensable means of information acquisition in fields such as remote sensing surveying and mapping, and disaster prevention and mitigation.

Initially, spaceborne SAR was employed for target identification and terrain mapping. For target identification applications, a single satellite proved insufficient to meet users' requirements for timely observation of disaster areas and moving targets due to a long revisit time. In response to this challenge, loosely coupled distributed spaceborne systems composed of identical spaceborne SAR payloads emerged. These satellites operated in the monostatic mode, running either on different orbital planes or on the same orbital plane with different phases [5]. An illustrative example is the COSMO-SkyMed mission proposed by Italy in 1998 [6]. Terrain mapping, accomplished using across-track interferometric (XTI) SAR, requires two SAR images with slightly different viewing angles to generate a Digital Elevation Model (DEM) [7]. Generally, for a single spaceborne SAR, it is realized by using repeated tracks or dual antennas on the platform. However, the accuracy of DEM measurements using these methods is constrained by either temporal decorrelation of scenes [8], atmospheric disturbances [9], or the maximum available baselines [7]. An effective solution is to organize two (or more) similarly designed SAR satellites to form a close formation with a baseline ranging from dozens of meters to a few kilometers in the cross-range direction, simultaneously or near-simultaneously acquiring echoes of the same region [10]. The first in-orbit close formation spaceborne SAR is the German TanDEM-X [11]. These two types of SAR configurations, composed of identical or similar SAR satellites, are referred to as *homogeneous* distributed spaceborne SAR systems in this review, as shown in Fig. 1.

With the driving force from remote sensing applications of multi-dimensional information retrieval, homogeneous distributed spaceborne SAR systems are progressing towards acquiring multi-angle observation capabilities [12]. The Earth Explorer-10 mission by the ESA, known as Harmony [13], represents a significant development in multi-angle formations. This multi-static SAR involves three satellites positioned hundreds of kilometers apart in its stereo mode to achieve simultaneous multi-angle observations. It is aimed to retrieve both the two-dimensional (2-D) velocity vector of ocean currents and three-dimensional (3-D) surface deformations.
Generally, spaceborne SAR can be classified by orbit altitude into Low Earth Orbit (LEO) SAR (altitude <1000 km), Medium Earth Orbit (MEO) SAR (altitude of 1000~36500 km), and Geosynchronous SAR (altitude of 36500 km). The advancement of space technology also facilitates the concept of homogeneous distributed spaceborne SAR systems deployed in geosynchronous (GEO) orbits [14]. For distributed GEO SAR, there are also loose formations such as Global Earth Satellite System (GESS) [15] and close formations like Geosynchronous SAR For Earth Monitoring by Interferometry and Imaging (GEMINI) [16]. These configurations aim to enhance revisit capabilities and mitigate atmospheric disturbances, respectively. Additionally, in recent years, GEO SAR systems incorporating multi-angle observations have been under study to achieve continuous 3-D surface deformation measurements in disaster-stricken areas [17].

As the number of available spaceborne SAR systems continues rising, bistatic SARs with radar satellites illuminating and ground-based or airborne platforms receiving has emerged as a crucial approach to enrich SAR data sources. In addition to

Published by IEEE. This is the Author Accepted Manuscript issued with: Creative Commons Attribution License (CC:BY 4.0).
The final published version (version of record) is available online at DOI:10.1109/mgrs.2025.3535412. Please refer to any applicable publisher terms of use.

utilizing Low Earth Orbit (LEO) SARs such as TerraSAR-X [18], Gaofen-3 [19], and Lutan-1 [20], a particularly noteworthy illuminator is GEO SAR [14]. With its high orbit at an altitude of nearly 36,000 km, the beam of GEO SAR easily covers the receiving regions of LEO satellites, aircrafts, and ground platforms, enabling the deployment of various types of receivers. Thanks to a revisit time of less than 24 hours, bistatic SAR systems utilizing GEO SAR as the illuminator have become a pivotal method for local, rapid, and continuous imaging and measurements. Furthermore, compared to spaceborne SAR, the quantity of in-orbit communication and navigation satellites holds a significant advantage. Consequently, establishing equivalent bistatic SAR systems by deploying passive receivers to collect reflected echoes from the scenes illuminated by these non-radar satellites proves to be an effective strategy for enhancing observation timeliness. Notable instances of such bistatic SAR configurations include the communication-GEO bistatic SAR proposed in 1998 [21] and the navigation-ground bistatic SAR proposed in 2002 [22]. These systems, characterized by significant differences in transmitting and receiving platforms, are denoted as *heterogeneous* distributed spaceborne SAR systems in this review. Heterogenous distributed spaceborne SAR systems include systems with radar-based and non-radar illuminator, depending on the types of transmitter, as shown in Fig. 1.

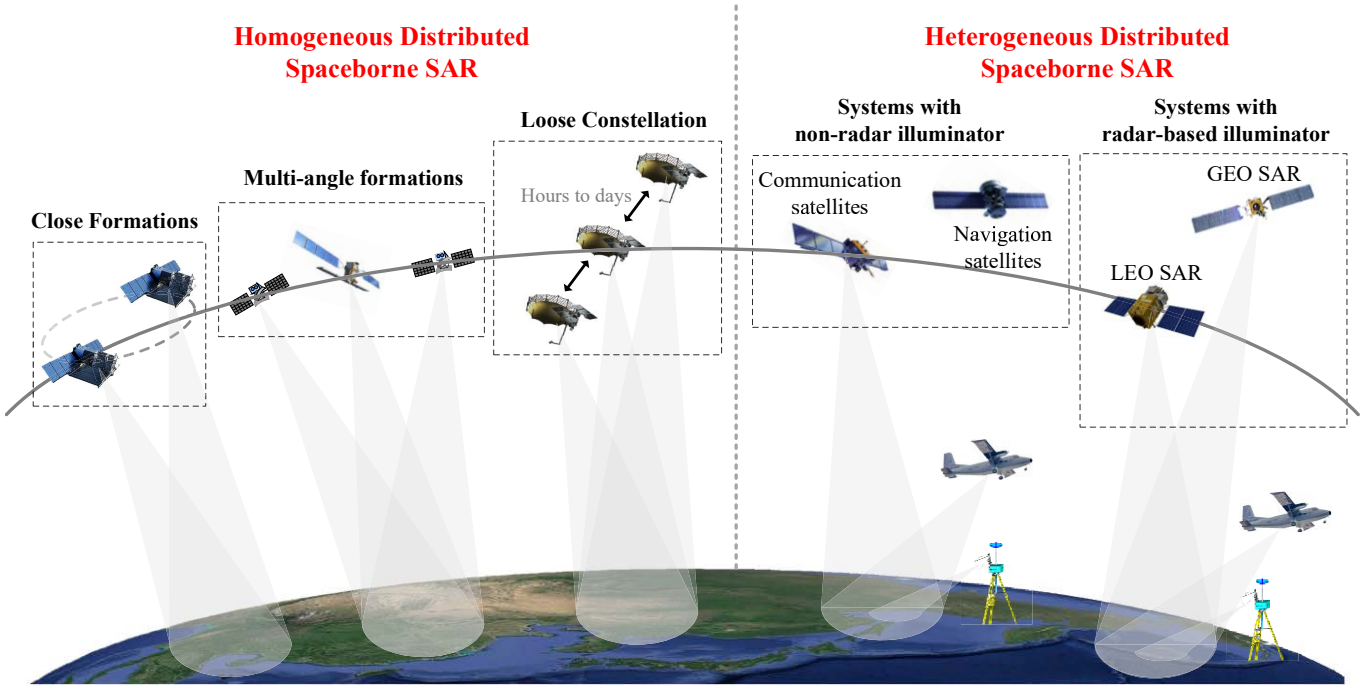

Fig. 1 Types of distributed spaceborne SAR. It is classified into homogeneous and heterogeneous distributed spaceborne SAR, depending on whether the transmission platforms and receiving platforms are identical/similar or not.

This review provides a comprehensive review of both homogeneous and heterogeneous distributed spaceborne SAR systems, encompassing their origins, developmental history, typical missions, and associated key technologies. Subsequently, the review delves into a discussion of representative applications of distributed spaceborne SAR, covering areas such as intelligent target recognition, terrain mapping, deformation retrieval, atmosphere measurements, and ocean observation. Finally, the review concludes by offering insights into the potential future developments of distributed spaceborne SAR systems.

II. Homogeneous Distributed Spaceborne SAR

A. Close formations

A typical application of spaceborne SAR is DEM mapping via Interferometric SAR (InSAR). In the early stages, spaceborne SAR relied on repeat-pass observation to measure DEM [23]. However, the long repeat time, spanning several tens of days, significantly degraded the coherence [24]. The primary objective behind the close formation distributed spaceborne SAR was to overcome the bottleneck encountered in the repeat-pass InSAR DEM measurements [25]. The hallmark of close formations lies in the sufficiently close spacing between satellites, enabling coherent processing of signals/images and proper interferometric baseline between satellites simultaneously. They are generally designed to operate in bistatic/multi-static mode. The earliest concept of close formation, known as the Cartwheel concept, was proposed by Didier Massonnet from the French Space Agency (CNES) in 1998 [25], composed of one master satellite with three passive receiving slave satellites.

Another purpose of close formations lies in Ground Moving Target Indication (GMTI) by the methods of along-track interferometric (ATI) processing, displaced phase center

antenna (DPCA), etc. A typical concept is the TechSat21 proposed by the U.S. in 1999 [26], which operates in an along-track formation, engaging in space-time adaptive processing to suppress ground clutter.

Recently, there has been extensive attention to close formations for multi-satellite joint high-resolution (HR) imaging, with the core concept being the utilization of multiple satellites for bandwidth synthesis. Typical systems include the frequency-division multiplexing SwarmSAR [27] and MirrorSAR for achieving high-resolution wide-swath (WS) images by resolving azimuth ambiguity [28].

In addition to LEO SAR, the concept of close formations also extends to GEO SAR, encompassing along-track formations for atmospheric estimation or to reduce synthetic aperture time, mitigating the impact of atmospheric phase screens [16], and cross-track formations enabling coherence-based tomography [29] or multi-baseline DEM inversion [30].

The typical close-formation missions and their concepts are outlined in Table I. Only TerraSAR-X/TanDEM-X (TSX/TDX), Tianhui-2 (TH-2), Lutan-1 (LT-1, in XTI mode), Hongtu-1 (HT-1), and Gaojing-2 are operational. The main applications of these five missions are focused on terrain mapping. The remaining missions are either under development or in conceptual stages.

TABLE I
Typical Close Formation Distributed Spaceborne SAR Missions.

Mission	Formation	No. of Satellites	Launch Time	Status	Country/Organization	Applications
TSX/TDX	Helix	2	2007/2010	Operational (extended)	Germany	Terrain mapping
TH-2	Helix	2	2019	Operational	China	Terrain mapping
LT-1 (XTI mode)	Helix	2	2022	Operational	China	Terrain mapping
HT-1	Cartwheel	1 + 3	2023	Operational	China	Terrain mapping
Gaojing-2	Helix	2 + 2	2022/2024	Operational	China	Terrain mapping
TSL/TDL	Helix	2	--	Under development	Germany	Forest structure & surface deformation
SwarmSAR	Along-track	N	--	Conceptual	Netherlands	HR WS imaging & terrain mapping
MirrorSAR	Helix	M + N	--	Conceptual	Germany	HR WS imaging & terrain mapping
PRECURSOR – ECO	Along-track	3	--	Under development	Spain	HR imaging
GEMINI	Along-track	1 + 3	--	Conceptual	Italy	Vapor mapping & surface deformation
ARGOS	Along-track	6 + 2	--	Conceptual	Italy	Fast imaging & emergency response

As listed in Table I, a typical representative of the close formation distributed spaceborne SAR is the German TSX/TDX, which is also the first operational close-formation mission [11]. The TanDEM-X mission was proposed by German Aerospace Center (DLR) in 2003, which leverages the single-pass close formation between TanDEM-X, a satellite akin to TerraSAR-X, and TerraSAR-X itself, to generate high-resolution global DEM [31]. Both satellites operate in the X-band, adopting a Helix configuration for formation, at an orbit height of 514 km with a repeat cycle of 11 days, as shown in Fig. 2(a). TanDEM-X was launched in 2010. In 2012 and 2013, two successive global DEM measurements were accomplished, with 66% of the regions achieving an accuracy better than 2 m and 89% of the regions attained an accuracy superior to 5 m. After several supplementary acquisitions to fill in gaps, DLR eventually released the WorldDEM product in 2016, achieving a grid resolution of 12 m [32]. Despite surpassing its theoretical design lifespan, TSX/TDX continues to operate smoothly.

(a) (b)

Fig. 2 The schematic diagram of two in-orbit close-formation distributed spaceborne SAR. (a) German TSX/TDX with twin satellites flying in a Helix formation [11]. (b) Chinese HT-1 with a master and three slave satellites flying in a cartwheel formation [33, 34].

Besides TDX/TSX, another X-band twin-satellite close-formation mission in orbit is TH-2, launched in 2019 [35]. TH-2 is capable of Digital Surface Model (DSM) measurements with an optimal grid spacing of 5 m [36]. TH-2 is positioned at

an orbit height of 500 km with a repeat orbit cycle of 19 days, and its positioning accuracy is comparable to the TanDEM-X [36]. For the first time, TH-2 introduced a dual-frequency (9.6 GHz and 9.44 GHz) imaging mode to solve the interferometric phase ambiguity [35]. Before and after the normal single-frequency data acquisition, dual-frequency imaging is conducted respectively, each yielding 5 km×5 km image pairs whose areas are adjacent to that of the normal image. The ambiguity number of the phase in main frequency is determined from the dual-frequency image of the overlapped area and to generate high-resolution and high-accuracy DEMs.

In addition to X-band close-formation SAR missions, the L-band, due to its penetration and high temporal coherence, is particularly suitable for deformation monitoring and has also received widespread attention. Currently, the only L-band close-formation SAR mission is the Chinese LT-1. LT-1 operates at an orbit height of 607 km with a repeat orbit cycle of 8 days [37]. It is an explicitly deformation monitoring-focused SAR constellation, which satisfies the requirements of disaster emergency response, land surveying, global forest resource surveying, biomass retrieval, etc. Additionally, it is able to achieve DSM measurements with a grid resolution of 25 m [38, 39], in its close-formation mission phase. LT-1 was successfully launched on January, 2022. Furthermore, LT-1 is the first multi-mode PolSAR system in China, supporting not only linear polarization but also compact polarization, mixed compact polarization, circular polarization, elliptical polarization, and code-based mixed polarization modes [40]. LT-1 adopted Nonlinear Frequency Modulation (NLFM) signals as the transmission signals for the first time [41]. Compared to traditional Linear Frequency Modulation (LFM) SAR with weighing processing, NLFM has the same sidelobe level performance, while its SNR is increased by 1.25 dB, and the equivalent power is increased by 28%.

Another typical but still in-development L-band close-formation distributed SAR is the TanDEM-L (TSL), which is a slave spaceborne SAR identical to TerraSAR-L (TDL) [42]. It was proposed in 2009. The constellation orbits at a height of 745 km with a repeat cycle of 16 days. TSL/TDL offers various geophysical products related to the biosphere, hydrosphere, cryosphere, and lithosphere [43]. In its close-formation stage, it can provide DEM with a 12 m resolution. In 2017, TanDEM-L was in its final evaluation stage at the German Federal Ministry of Education and Research [38, 44].

To extend the applications or improve the performance of close-formation distributed SAR, missions encompassing three or more satellites have been proposed, and, eventually there is now a mission in orbit, the X-band HT-1 of China. HT-1 is the first in-orbit mission in the world that employs a Cartwheel formation, operating in the multi-static mode at a height of about 500 km, as shown in Fig. 2(b). With one master and three slave satellites, each single pass yields four sets of observational data, thereby meeting the requirements for high-precision DEM measurement and even tomographic imaging. In March 2023, the HT-1 was successfully launched. Currently, it has been deployed in various fields including topographic mapping, flood monitoring, geological hazard monitoring, and deformation monitoring [33, 34].

Other representative close formations include MirrorSAR proposed by DLR, SwarmSAR proposed by Delft University of Technology (TU Delft), and PRECURSOR-ECO proposed by National Institute for Aerospace Technology (INTA) of Spain. A notable feature of MirrorSAR is that one high-power payload is solely responsible for transmitting waveforms, while several low-power platforms are solely responsible for receiving echoes and relaying them to the main satellite [45], as illustrated in Fig. 3 (a). This design facilitates high-resolution wide swath imaging, single-pass multi-baseline interferometric imaging and tomography [46]. The S-band SwarmSAR [27, 47] is aimed to construct various flexible and higher-quality products through the collaboration of multiple small-size, low-cost SAR nodes, as shown in Fig. 3 (b). A notable application of SwarmSAR is synthesizing high-resolution images from individual satellites by utilizing Frequency Division Multiplexing (FDM) technology, thereby achieving a signal-to-noise ratio (SNR) enhancement of N^2, N being the number of satellites. The PRECURSOR-ECO [48] being developed consists of three identical X-band small satellites. It offers three collaborative working modes: wide-swath imaging, multi-baseline interferometric mapping, and high-resolution spotlight imaging. It has the same orbit height as TerraSAR-X. The constellation is expected to generate a 3 m resolution DEM of Spain in less than 90 days.

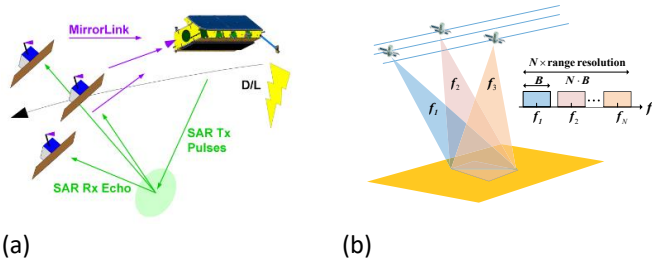

Fig. 3 The schematic diagram of (a) MirrorSAR [45], (b) SwarmSAR [47]. The FDM technology is expected in SwarmSAR, where N sub-bands with bandwidth B at frequency $f_1, f_2, \cdots, f_N$ can be synthesized into a large bandwidth up to $N \cdot B$.

In addition to the aforementioned LEO closely coupled formation distributed SAR, close formation GEO SAR has also received extensive attention. Due to the slow angular velocity deriving from the high altitude of GEO SAR, the integration time of a single GEO SAR is much longer than LEO SAR, typically several minutes to several hours, depending on orbit parameters and orbital positions [49, 50]. Therefore, the focusing of GEO SAR echo suffers from serious atmospheric phase errors.

A major objective of close formation GEO SAR is to mitigate the effects of atmosphere on the echo focusing of monostatic GEO SAR. Typical concepts include Geosynchronous SAR for Earth Monitoring by Interferometry and Imaging (GEMINI, in 2012) [51] and Advanced Radar Geosynchronous Observation System (ARGOS, in 2015) [52], both proposed by researchers from Politecnico di Milano (POLIMI).

The key idea of GEMINI is to use one or multiple pairs of close-range quasi-stationary GEO receivers to passively collect echoes from one X or Ku band GEO SAR satellite. This allows for the along-track interferometry with intervals of a few minutes to generate gradients of atmospheric delay that can be compensated for during the imaging over a long aperture time, as shown in Fig. 4. GEMINI can achieve continuous coverage coarse-resolution imaging with a 20-minute synthetic time and also high-resolution imaging utilizing a 6-hour synthetic time, which can be used for high spatiotemporal mapping of water vapor and daily deformation measurements [51].

ARGOS consists of multiple transmitting and receiving satellites aligned along the track, planned to operate in the C-band and X-band [52], as shown in Fig. 4. The major advantage of ARGOS lies in the significant reduction in antenna size and power budget per satellite compared to single high-inclination satellite schemes. For example, considering a resolution of 10 × 10 m, in the design with 6 transmitting satellites and 2 receiving satellites, the average power budget decreases from 24 kW to 0.5 kW per satellite, and the antenna area decreases from 350 m^2 to 33 m^2 per satellite [52].

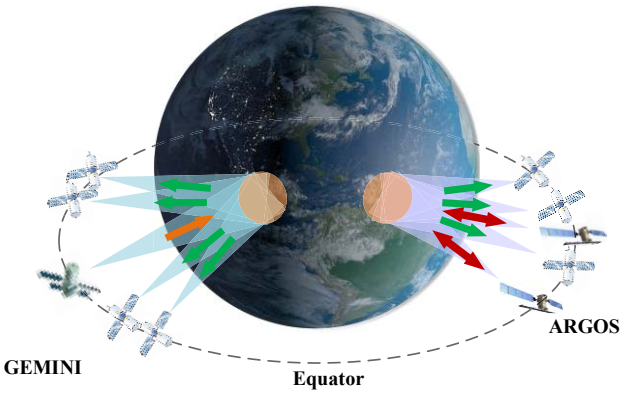

Fig. 4 Typical concept diagram of GEO SAR close formation. GEMINI is single-input multi-output system with one or more pair of receive-only payloads to achieve along-track interferometry. ARGOS is a multi-input multi-output system to synthesize a high-resolution SAR image with reduced integration time.

Although the close-range formation distributed spaceborne SAR systems vary in orbit height, configuration, and applications, they share numerous common technological aspects, including formation configuration design, inter-satellite synchronization, inter-satellite baseline measurement techniques, and some other innovative technologies.

1) Formation configuration design. The formation configurations, which directly relate to the baselines of the close formation systems, are important to determine the application performance. Cartwheel, Pendulum, and Helix formations are three important formations in the close formation distributed spaceborne SAR systems [53]. In the Cartwheel mission, there is no cross-track component. Several slave satellites orbit around a central point, rotating within the orbital plane. Therefore, perpendicular baselines are only contributed by radial baselines. However, due to the coupling between the radial baseline and the along-track baseline, there are also relatively long along-track baselines between satellites at certain latitudes, which lead to significant Doppler decorrelation in interferograms. Nevertheless, HT-1, which is a typical Cartwheel configuration, employs independent zero Doppler steering, ensuring a maximum Doppler coherence under a certain SNR loss and retaining multi-baseline interferometry capabilities [11]. On the contrary, in the Pendulum formation [54], the slave satellite moves only in the cross-track direction, and the along-track baseline is fixed to reduce Doppler decorrelation, resembling a pendulum motion with pivot at the master satellite.

However, both the Cartwheel and Pendulum formation have a significant orbital variant effective baseline. To address the issue, Helix configuration is a good option, which utilizes different Right Ascension of Ascending Node (RAAN) and eccentricity vectors to provide cross-track and radial baselines respectively [55]. It has a relatively stable effective baseline. Additionally, this configuration ensures that neither the along-track nor cross-track baselines are simultaneously zero, thus mitigating collision risks. The Helix configuration is currently the most widely adopted one. TanDEM-X, TH-2, LT-1, Gaojing-2, and the yet-to-be-launched TanDEM-L all employ this configuration.

For GEO SAR close formations, the effects of Earth rotation on baseline components cannot be neglected, therefore, it is necessary to design the formation with the consideration of the effects of the Earth's rotation [56]. In this case, the effective cross-track baseline is contributed by both the cross-track and along-track baselines in the Earth-centered inertial (ECI) frame. Leveraging the ECEF frame Relative Motion Equations (RMEs), researchers have designed GEO SAR formations with twin satellites, which can be used for single-pass DEM measurements and repeat-pass tomographic imaging. Different from the formation for DEM measurements, the formation for repeat-pass tomographic imaging requires that the master and slave satellites have slightly different semi-major axes [29]. Giving the master and slave different semi-major axes means that they drift steadily apart (they no longer have the same orbit period). Typical formations are shown in Fig. 5

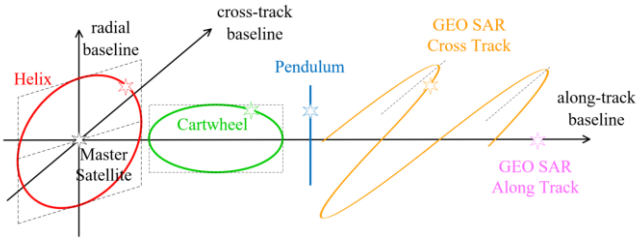

Fig. 5 Typical formation in close-formation distributed spaceborne SAR, where the motion of the slave satellite is relative to the master satellite (at the origin).

2) Inter-satellite synchronization. Bistatic/multi-static distributed spaceborne SAR requires synchronization, which includes space synchronization, time synchronization, and phase synchronization. Current in-orbit close formations utilize independent zero Doppler steering instead of joint azimuth footprint [11]. Considering both Doppler decorrelation and SNR loss, the former provides a higher interferometric

coherence. However, for GEO SAR close formations, rotational decorrelation needs to be considered due to unparallel trajectories between satellites [57]. Therefore, the independent zero Doppler steering is no-longer optimal, and trajectory needs to be considered to fine-tune the beam steering direction of the slave satellite [58].

Time synchronization typically involves triggering of data acquisition and time drift correction during data acquisition. Existing bistatic distributed spaceborne SAR systems generally use pulse per second (PPS) signals to trigger data acquisition. The accuracy of triggering in TanDEM-X is 1-2 μs [10]. The drift correction (mainly induced by constant frequency difference between satellites) will lead to a drift of the receiving window. TanDEM-X adopts a leap pulse repetition frequency (PRF) to compensate for it, where the frequency difference between the two satellites estimated through inter-satellite synchronization pulses [59] serves as a priori. The time synchronization error of TanDEM-X is better than 5 μs within a working time of 10 minutes [60]. Whereas both TH-2 and LT-1 adopt disciplined high-stability oscillators to correct time drift. TH-2 uses a rubidium clock with a long-time high stability to discipline the crystal oscillator, while LT-1 uses Global Positioning System (GPS) to discipline the rubidium clock oscillator. The time error of LT-1 can be limited to within 60 ns during a 10-minute data acquisition [60].

Inter-satellite synchronization pulses are the most widely applied technology for phase synchronization in operational close-formation bistatic distributed spaceborne SAR. Traditional scheme requires the normal work, i.e., the radar signal transmitting and echo receiving, to be interrupted, as shown in Fig. 6(a). This scheme is adopted in TanDEM-X and TH-2. Whereas LT-1 adopts a novel scheme where the phase synchronization signal is exchanged by virtue of a time slot between radar signals, so data acquisition is not interrupted [60], as shown in Fig. 6(b). The phase synchronization accuracies of TanDEM-X, TH-2, and LT-1 are 1° [10], 6.28° [35], and 0.3° [60] respectively.

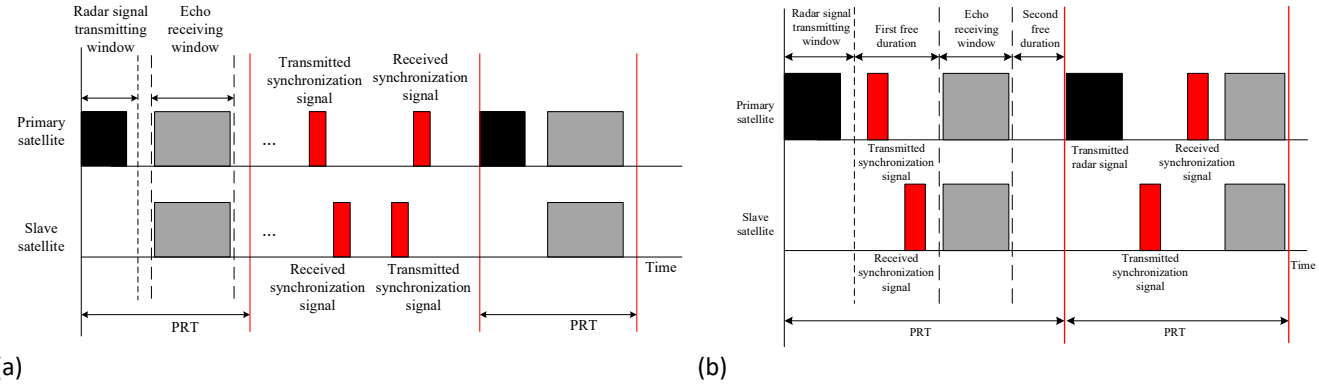

Fig. 6 Two typical phase synchronization schemes. (a) The interrupted scheme. (b) the non-interrupted scheme (revised from [60]).

3) Inter-satellite baseline measurement. To precisely measure the inter-satellite baseline between the satellites in the formation, dual-frequency Global Navigation Satellite System (GNSS) receivers are adopted in all satellites of operational close formation distributed spaceborne SAR, enabling differential GNSS technology. TanDEM-X is equipped with GPS receivers (Integrated GPS Occultation Receiver, IGOR), achieving a baseline measurement accuracy of up to 1 mm [61, 62]. TH-2 is compatible with GPS and Chinese Beidou-2 (BD-2), with a 3-D baseline measurement accuracy within 2 mm.

B. Multi-angle formations

Different from close formations, in a multi-angle formation distributed spaceborne SAR, the distance between satellites exceeds the critical baseline for coherent synthesis or interferometry, but the satellites have a common beam footprint. The merits of multi-angle formation distributed spaceborne SAR are capability of measuring bistatic/multi-static scattering characteristics with large bistatic angle, and rich diversity in line of sight (LOS) observations. Such advantages enable it to map the vegetation terrain and measure the vector parameter such as 3-D surface deformation.

Multi-angle formations have been receiving significant attention from the ESA in the past decade, with typical missions including SAOCOM Companion Satellite (SAOCOM-CS), SEntinel-1 SAR Companion Multistatic Explorer (SESAME), and Harmony [13]. SAOCOM-CS proposed in 2014 offers three configurations [63], including the tomographic configuration (for forest and ice structure), bistatic configuration (for urban deformation and vegetation scattering), and specular configuration (for soil moisture), as shown in Fig. 7(a). SAOCOM-CS was originally planned to be launched simultaneously with SAOCOM-1B in 2019, but the mission was canceled. SESAME, proposed in 2016, is a proposal in ESA's Earth Explorer (EE)-9 mission [12]. It involves two passively receiving satellites flying with Sentinel-1, separating about 200 km in the along-track direction. The two satellites are organized in a close formation to achieve single-pass interferometry, as shown in Fig. 7(b). The primary applications of SESAME include terrain measurement, surface deformation, and biogeophysical parameter retrieval.

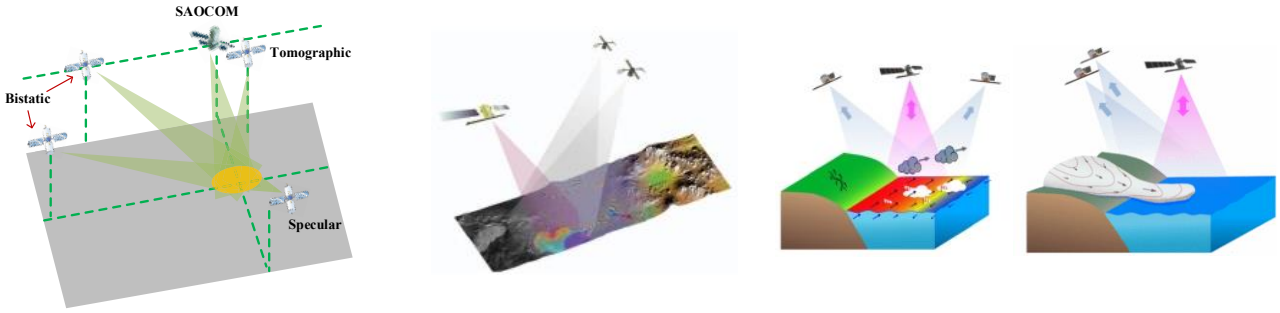

(a) (b) (c)

Fig. 7 Typical multi-angle formations in distributed spaceborne SAR. (a) SAOCOM-CS. (b) SESAME [12]. (c) Harmony [64].

Inherited from SESAME, Harmony (initially named STEROID) has a stereo phase apart from XTI phase, as shown in Fig. 7(c). Harmony aims to provide enhanced radar observations of the ocean, cryosphere, and solid Earth, with both scientific and engineering significance [13, 65]. In 2022, Harmony was finally selected as the only ESA Earth Explorer 10 (EE-10) mission candidate entering into the Phase B1 stage [64], and it is expected to be launched in 2029. The overall mission is designed to last for five years, as shown in Fig. 8. The most significant feature of Harmony is its stereo phase [13] where the two companion passive satellites, Harmony-A and Harmony-B, are 350-400 km ahead and behind the master satellite, respectively. Combined with the master satellite Sentinel-1D, three independent LOS can be provided. Benefiting from the observation angle diversity, the most featured application of Harmony is the measurements of surface parameter vector, such as the ocean surface wind vector, Total Surface Current (TSC) vector, and the 3-D Velocity (TDV) vector of the solid Earth. Measuring parameter vectors of the ocean is a novel application which is hardly mentioned in the previous spaceborne SAR missions. Fig. 9 shows a typical example of the parameter vector measurements of the Harmony on the ocean. The standard deviation of the estimation error in the across-track and along-track components are about 0.03 m/s and 0.08 m/s, respectively. The accuracy of another notable application, the TDV of the solid Earth by using multi-angle differential interferometric SAR (D-InSAR) methods, generally meets the threshold requirements 2 mm/yr.

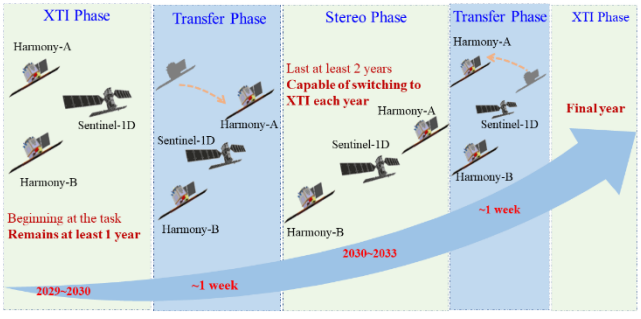

Fig. 8 Life cycle planning of Harmony, which includes two years of XTI phase (baseline 400 m ~ 1 km) and two years of Stereo phase which can occasionally switch to XTI formation.

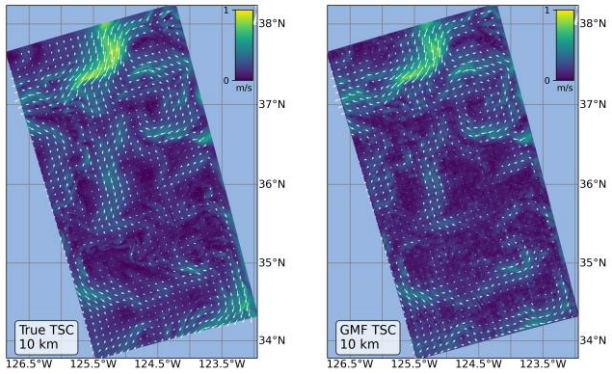

(a) (b)

Fig. 9 A simulation example of the parameter vector measurement by the Harmony mission [65]. (a) Input TSC vectors for simulation. (b) Estimated TSC vectors.

A key technology of Harmony is the phase and time synchronization between Harmony and the radar transmitter on Sentinel-1, where the distance between them is much larger than the close-formation systems [65-70]. Instead of mutual synchronization pulses applied in TanDEM-X, Harmony employs Ultra Stable Oscillator (USO) clocks on all spacecraft and GNSS receivers to correct frequency and phase errors. The common-clock approach, whereby the GNSS receivers are linked with the SAR instrument USO clock, enables the GNSS receivers to retrieve any drift between local clocks and the atomic clock reference of the GNSS system. For the so-called coarse-time synchronization, precise orbit of the Sentinel-1 is determined and the position corresponding to data acquisition start time is predicted. This information is uploaded to the Harmony from the Sentinel-1 ground segment prior to data acquisition to determine a coarse time for data acquisition. Finally, the fine-time synchronization is achieved by echo tracking method whereby the actual received echo is correlated on board with expected echo. This echo tracking can already be performed on the sequence of warm-up pulses used by Sentinel-1 before the start of the data take. The accuracy of phase, coarse-time, and fine-time synchronization are better than 5°, 3 ms, and 50 μs, respectively. Another critical challenge in interferometric processing of Harmony is that conventional monostatic definition of interferometric parameters, including temporal lag, sensitivity, and spectral shift, becomes opaque in complex bistatic configurations. This issue can be addressed by the wavenumber domain support in [71].

C. Loose Constellation

Although revisit times can be reduced through specialized imaging modes such as ScanSAR and TOPS (Terrain Observation by Progressive Scans) [72], a common solution to improve the revisit time and repeat-pass time is to use more satellites and enable each satellite to observe the same scene at distinct time intervals. Such constellation is referred to as loose constellation. The first SAR constellation is the Onyx (formerly known as Lacrosse) of the U.S., which encompasses five satellites, with its first one launched in 1988 [73] [74]. From 2006 to 2022, Germany, Italy, ESA, Canada, and China have each launched their own SAR satellite constellations, exemplified by SAR-Lupe [75], COSMO-SkyMed [6], Sentinel-1 [76], Radarsat Constellation (RCM) [77], and GF-3 [78]. During this era, the number of satellites in each constellation ranges from two to five satellites, and most constellations are each arrayed on a single orbital plane (SAR-Lupe has three orbital planes [79]). Different from other constellations like Radarsat Sentinel-1, LT-1 (in its repeat-pass mode), and SAOCOM [80], the four satellites of the Italian COSMO-SkyMed are distributed non-uniformly, resulting in a non-uniform repeat time, which is 8, 3, 4, and 1 day [81].

In addition to the LEO SAR constellation, there is also a GEO SAR constellation, the Global Earthquake Satellite System (GESS), proposed by the U.S. in 2003. It encompasses 10 GEO SAR satellites divided into five groups to cover the whole globe [15]. The two satellites in each group are separated by a 180-degree phase, allowing for deformation measurements with a repeat-pass time of 12 hours. However, due to financial constraints, the GESS project was put on hold. Typical loose constellations of spaceborne SAR are shown in Table II.

Since 2018, there has been an explosion in large-scale SAR constellations. Such large-scale constellations composed of miniaturized satellites have become a research hotspot and a key development direction. The U.S. and Finland launched the first satellite of the Capella [82] and ICEYE constellations [83] in 2018, while Japan and China launched the first satellite of StriX-α/β/1 [84] and Tianxian [85] in 2020 and 2022, respectively. In particular, China is engaged in the active development of miniaturized SAR satellites, with Haisi-1 [86], Qilu-1 [87] and Chaohu-1 [88] launched in 2020, 2021, and 2022, respectively, as shown in Fig. 10.

(a) (b) (c)

Fig. 10 Mini-satellite SARs launched by China. (a) Haisi-1 [86], (b) Qilu-1 [87], (c) Chaohu-1 [88].

TABLE II
Typical Spaceborne SAR Loose Constellations

Mission	Satellite Number	Launch Time	Status	Country /Organization	Applications
GESS	10	--	Conceptual	USA	National security, emergency Ocean and coastal observation
COSMO-SkyMed	4	2007	Operational (extended)	Italy	Civil and Military
SAR-Lupe	5	2006	Operational (extended)	Germany	Reconnaissance and emergencies
Radarsat Constellation	3	2019	Operational	Canada	Reconnaissance
Sentinel-1	2	2014	Operational	ESA	Maritime surveillance Monitoring emergencies and ecosystem
GF-3	3	2016	Operational	China	Marine environment surveillance Monitoring sea ice, land surface motion risks
LT-1 (DM mode)	2	2022	Operational	China	Disaster monitoring, water conservancy, maritime and meteorology
SAOCOM	2	2018	Operational	Argentina	Disaster monitoring
ICEYE	18	2018	Operational	Finland	Monitoring geohazard
Capella /Acadia	36	2018	Operational	USA	Natural catastrophes, security and environmental monitoring
Lacrosse	3	1988	Out of Production	USA	High resolution SAR imagery
Tianxian	96	2020	Under development	China	Reconnaissance
StriX-α/β/1	25(StriX)	2020	Operational	Japan	Monitoring land, disasters and geohazards and the cryosphere

TABLE III
Comparison of Key Parameters Between TerraSAR-X And Typical Miniaturized Satellites

Mission	Weight (kg)	Antenna size	Polarization	Peak-power(kW)	Max. Bandwidth(MHz)	Incident angle(°)	NESZ (dB)	Azimuth resolution (m)/ width(km) (Stripmap mode)	Design life
TerraSAR-X	1230	4.8×0.7	fully polarized	2.26	150	15~60	≤-19	3.3/30	5 (more than 16 years actually)
ICEYE	85	3.2×0.4	single polarization	4	300	10~35	<-17	3/30	3
Capella	116	diameter 3.5	single polarization	0.6	500	25~40	--	1.2/5	3
StriX	150	4.9×0.7	single polarization	0.1	300	15~45	≤-15	3/30	--

Fig. 11 Typical in-orbit homogeneous distributed spaceborne SAR missions as of May 2024.

Large-scale constellations are in general distributed across multiple orbital planes to significantly reduce the repeat-pass and revisit time. These miniaturized satellites generally have a simpler design compared to traditional spaceborne SAR. Taking the X-band spaceborne SAR as an example, the key parameters of the TerraSAR-X and the miniaturized satellites ICEYE, Capella-X and Stirx are compared in Table III. It can be observed that miniaturized spaceborne SAR systems have a significant reduction in weight and power consumption while maintaining a similar level resolution compared to traditional missions. As a summary, such miniaturized spaceborne SAR systems have the following characteristics:

(1) *Dedicated to high-resolution imaging*. Most of the miniaturized SAR systems are in X-band (Chinese missions also employ C or Ku band), with a bandwidth of over 300MHz, offering a resolution of 1 m or even sub-meter level.

(2) *Simplified satellite design*. Miniaturized SAR systems are generally designed with single polarization and smaller incidence angle range. Additionally, the Noise Equivalent Sigma Zero (NESZ) is usually a bit worse than traditional missions.

(3) *Developing towards low-cost large-scale constellations.*

The satellites in miniaturized SAR systems often utilize mature and highly integrated commercial technologies. They are designed for rapid iteration instead of pursuing longer lifespans. With this idea, large-scale constellations can be achieved.

Fig. 11 shows typical in-orbit distributed spaceborne SAR missions. Note that some missions have been extended, e.g., SAR-Lupe and COSMO-SkyMed.

III. Heterogeneous Distributed Spaceborne SAR

A. Systems with radar-based illuminator

LEO, MEO and GEO SAR can all serve as illuminating sources for heterogeneous distributed spaceborne SAR. Currently, research predominantly focuses on using LEO SAR and GEO SAR as illuminating sources.

Heterogeneous distributed spaceborne SAR systems using LEO SAR as the illuminating source include spaceborne-airborne bistatic SAR (SA-BSAR) [89] and space-surface bistatic SAR (SS-BSAR) [20]. Due to the long repeat-pass time of LEO SAR, typically more than several days, research on LEO SAR-based heterogeneous distributed spaceborne SAR is usually aimed at principle verification. Currently, there have been many public experiments of SS-BSAR [90]-[91], where the experiments typically include imaging [92-95], DEM generation, and, more recently, repeat-pass D-InSAR [82, 96]. However, due to the relatively high cost and technical challenges of airborne tests, there are fewer experiments on SA-BSAR, and they typically focus on imaging tests [92-95], with few interferometry and tomography tests.

The earliest SA-BSAR experiment was conducted by National Aeronautics and Space Administration (NASA) in the 1980s using the Space Shuttle Challenger as the transmitter with CV-990 aircraft as the receiver [97]. This experiment produced bistatic images with resolution of approximately 20 m over Sioux City, Iowa, validating the feasibility of SA-BSAR [98]. Two other SA-BSAR experiments were conducted by NASA in 1990s utilizing the ERS-1 as the illuminator [99, 100], where the relationship between the resolutions and the bistatic geometry was demonstrated. From 2007 to 2009, DLR and Fraunhofer Institute for High Frequency Physics and Radar Techniques (FHR) carried out a series of SA-BSAR imaging experiments based on TerraSAR-X, F-SAR, and PAMIR [33, 34, 101-104]. Strip mode and reverse sliding spotlight mode were adopted to collect echoes. The comparison of monostatic and bistatic SAR images is shown in Fig. 12. It can be observed that there are obvious differences in target scattering characteristics between monostatic and bistatic SAR images. In 2020, the University of Electronic Science and Technology of China (UESTC) cooperated with the China Academy of Space Technology (CAST) to carry out the first Spaceborne-airborne bistatic SAR imaging test in China, using GF-3 as the illuminator [19].

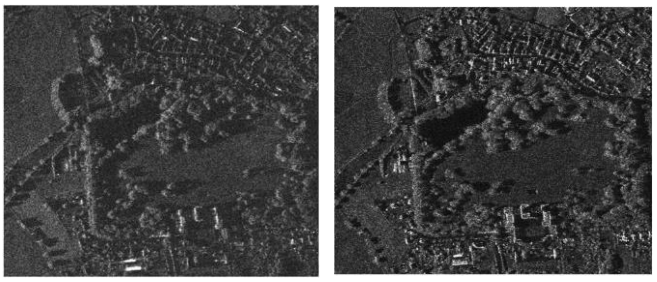

(a) (b)

Fig. 12 Classical SA-BSAR experiment results. Comparison of monostatic and bistatic SAR images. (a) SA-BSAR image [34] with TerraSAR-X as illuminator. (b) Monostatic TerraSAR-X image for comparison [34].

In terms of SS-BSAR, in 2006, researchers from Polytechnic University of Catalonia (UPC) developed a C-band receiving system, SARBRINA. They conducted the first SS-BSAR experiment where SARBRINA was employed to receive the signal from ENVISAT [94, 95]. From 2008 to 2010, they carried out many SS-BSAR experiments based on the ERS-2 satellite, including the first single-pass InSAR [105, 106], first repeat-pass InSAR [107], and the first transponder-based tomographic SAR (TomoSAR) [108]. In 2009, researchers from the University of Siegen used the TerraSAR-X with dual-pol mode as the illuminator and finally obtained the first polarimetric SS-BSAR image [109]. Subsequently, from 2009 to 2022, researchers from the University of Siegen [109-112], Politehnica University of Bucharest (PUB) [75, 93, 113-120], Sandia National Laboratories (SNL) [121], Beijing Institute of Technology (BIT) [91, 122-126], Institute of Electronics, China Academy of Science (IECAS), the National University of Defense Technology (NUDT) [127], and UESTC [128] have successively conducted SS-BSAR experiments, where the processing covering imaging, InSAR, TomoSAR etc. The illuminators used for experiments include TerraSAR-X, Sentinel-1, COSMO-SkyMed, GF-3, LT-1, etc.

Recently, research on D-InSAR and TomoSAR, which were typically carried out by researchers from PUB and BIT, have become a hot topic in SS-BSAR. In 2017, researchers from PUB developed an opportunistic C-band bistatic SAR differential interferometry architecture (COBIS), and demonstrated the opportunity and performance of repeat-pass C-band SS-BSAR with Sentinel-1 as the illuminator [75]. Results from several months of experiments showed that thanks to scanning from different sub-swaths from the Sentinel-1, the echo may be divided into several discontinuous segments in the azimuth direction, and furthermore, two different incident angles, among which one was achieved via the elevation sidelobes of Sentinel-1 beam. The experiment also retrieved deformation of a plaza, showing that the measured deformation kept with the temperature variation, as shown in Fig. 13. Results from the transponders show that the short-term and long-term deformation accuracies reached approximately 1 mm and 2 mm, respectively. In 2021, they developed another system, TomoSAR-1B, with which a tomographic imaging experiment of two transponders was carried out, demonstrating that a sub-meter height accuracy can be obtained under the

condition of signal-to-clutter ratio (SCR) higher than 28 dB [113, 129].

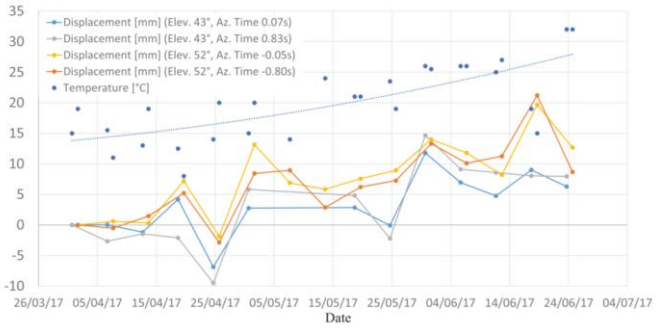

Fig. 13 Displacement time series [mm] of the observed plaza building and the temperatures [°C] at the dates of acquisition [75].

In 2022-2023, BIT conducted several SS-BSAR experiments using the Chinese LT-1 as the illuminator, involving InSAR, D-InSAR and TomoSAR processing for a 3 km × 3 km area, as is shown in Fig. 14. They reconstructed single-pass and repeat-pass DEMs with an accuracy of meter level [75, 130]. Subsequently, D-InSAR deformation map with a centimeter-level accuracy was retrieved, demonstrating the D-InSAR deformation measurement capability of L-band SS-BSAR. Recently, using 11 repeat-pass SS-BSAR images with a baseline span of approximately 2 km, they performed tomographic processing on an area of about 600 m × 600 m, generating 3-D urban point clouds with an accuracy of about 3.5m [131].

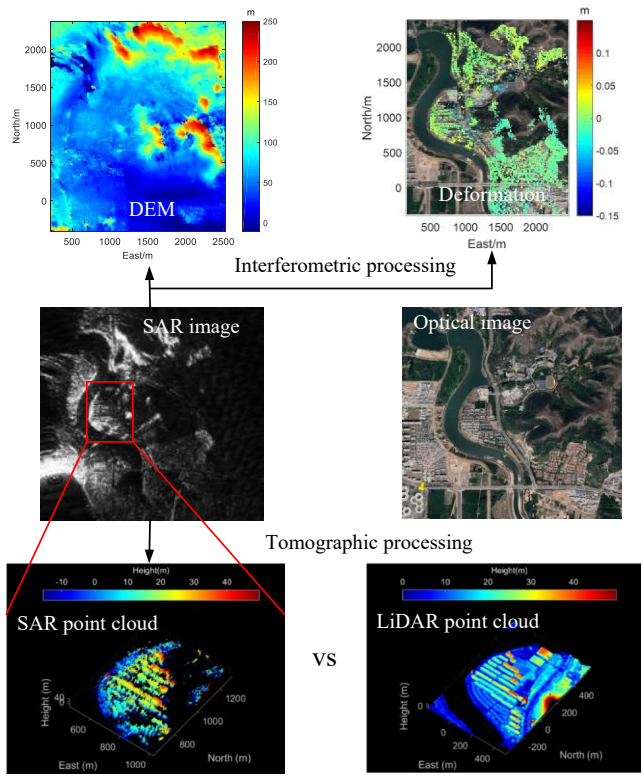

Fig. 14 Recent progress of SS-BSAR experiments carried out by BIT. The DEM and deformation were retrieved via single-pass and repeat-pass interferometric processing, respectively. The SAR point cloud was reconstructed by repeat-pass tomographic processing. As a comparison, LiDAR point cloud was mapped.

The heterogeneous distributed spaceborne SAR utilizing GEO SAR as the illuminator includes GEO-LEO bistatic SAR (BSAR) [132] and GEO SA-BSAR [133, 134]. For GEO-LEO BSAR, research is focused on the coherent synthesis of multiple images for resolution enhancement [135], whereas the major research of GEO SA-BSAR is imaging and moving target detection (MTD) [136, 137]. The concept of GEO-LEO BSAR and GEO SA-BSAR were both proposed by the MITRE Corporation from the U.S. firstly [138], whereas currently, most active researchers are from China. In GEO SA-BSAR, since the angular velocity of GEO SAR is much lower than that of the aircraft, multiple azimuth channels are generally required for the receiving antenna to solve the ambiguity [139]. Theoretical research in this area is quite extensive [140], whereas there have been no published practical experiments yet, as the first GEO SAR was just launched in August 2023 [141]. Typical experiment of the heterogeneous distributed spaceborne SAR with radar-based illuminator are listed in Table IV.

The key technologies of heterogeneous distributed spaceborne SAR systems with radar-based illuminator include configuration design, imaging methods, synchronization technology, and MTD processing.

The configuration design in heterogeneous spaceborne SAR systems mainly refers to optimizing the flight direction and beamsteering direction of the receiver, as the illuminator generally has an independent task. Research on configuration design primarily focuses on the systems with GEO SAR as the illuminator. The metrics under consideration mainly include 2-D resolution, SNR, and coverage capability, etc. For GEO SA-BSAR, both stationary area scenes and moving targets have been considered for configuration design [97, 142], whereas only stationary area scene was studied in GEO-LEO BSAR [143]. In particular, there are also studies focusing on problems in the design of Unmanned Aerial Vehicle (UAV) flight path planning [144-146] in GEO SA-BSAR. Due to extensive search space led by the numerous receiver parameters to be optimized, numerical optimization methods, represented by the Non-dominated Sorting Genetic Algorithm (NSGA) that is suitable for multi-objective optimization [147], are generally used by researchers to solve configuration design problems.

TABLE IV
Typical Experiment of The Heterogeneous Distributed Spaceborne SAR Utilizing SAR as The Illuminator

Illuminator	Receiving Platform	Time/ Institution	Significance
Space Shuttle Challenger	CV-990 Aircraft	1980s/NASA, U.S.	Verifying feasibility of SA-BSAR imaging
TerraSAR-X	F-SAR Aircraft	2007/DLR, Germany	Verifying SA-BSAR imaging using X-band spaceborne SAR
TerraSAR-X	PAMIR	2009/FHR, Germany	Verifying SA-BSAR for double sliding spotlight mode
GF-3	Aircraft	2020/UESTC, China	Verifying SA-BSAR imaging using Chinese spaceborne SAR
RADARSAT-1	Ground-based	2003/CCRS, Canada	Verifying SA-BSAR imaging
ENVISAT	Ground-based	2005/UPC, Spain	Verifying InSAR in single-pass SA-BSAR
YaoGan-10	Ground-based	2012/BIT, China	Verifying single-pass interferometric SS-BSAR using Chinese spaceborne SAR
COSMO-SkyMED	Ground-based	2013/SNL, USA	Verifying change detection from SS-BSAR
TerraSAR-X	Ground-based	2015/IECAS, China	Verifying SS-BSAR for staring- spotlight mode
GF-3	Ground-based	2020/UESTC, China	Verifying SS-BSAR imaging using C-band Chinese spaceborne SAR
LT-1	Ground-based	2022/BIT, China	Verifying single-pass interferometric SS-BSAR using L-band Chinese spaceborne SAR

As for imaging methods, they diverge significantly between different geometries. The accurate range history, as the basis of imaging, is generally modeled as the sum of the transmitter range and receiver range. For LEO SAR with short Synthetic Aperture Time (SAT) and the aircraft, it is accurate enough to adopt the Hyperbolic Range Equation (HRE) model. However, for LEO SAR with long SAT and GEO SAR, HRE is no longer accurate, thus, improved HRE with additional terms, or the polynomial range model can be applied. Regarding modeling the spectrum analytically, the series reversion stands as a universal method. In certain geometries where the angular velocity of one platform vastly surpasses that of the other, the bistatic geometry can be effectively considered as a monostatic one. For the frequency domain imaging algorithms, the Nonlinear Chirp Scaling (NCS) algorithm is the one most widely applied [148]. Given the more serious range-azimuth coupling in LEO SA-BSAR, researchers have combined the NCS with other techniques such as Scaled Inverse Fourier Transform (SIFT), Non-Uniform Fast Fourier Transform (NUFFT) [149]. For GEO SA-BSAR, ambiguity mitigation is in general taken into consideration to combine with NCS algorithm. In case of maneuvering platforms, conventional range history model cannot be applied, thus time-domain imaging algorithms like the Fast Factorized Back-Projection (FFBP) [150] are good options robust for most scenarios.

In the term of synchronization, since the beam footprint of the illuminator is generally much larger than that of receiver, it is easy to achieve space synchronization by simply deploying the receiver (airborne or ground-based receiver) inside the coverage area of the speceborne SAR illuminator. For time and phase synchronization, since the illuminator typically occupies a higher platform than the receiver, the most common method is the utilization of direct wave [151]. The receiving platform can estimate the signal arrival time based on the envelope of the direct wave, and phase synchronization can be straightforwardly accomplished by compensating the echo with the extracted synchronization phase from the direct wave, or directly by performing pulse compression on the echo using the direct wave as a reference function [152].

MTD is a distinctive application in GEO SA-BSAR, whereas other heterogeneous distributed spaceborne SAR systems are deemed not suitable for MTD due to excessively high or low platform velocities or insufficient coverage time. The first research focus in this field is Doppler ambiguity suppression. Primary ideas to suppress the Doppler ambiguity are to construct spatial filter from multiple azimuth channels, and thus, to reconstruct multi-channel signals [153, 154]. In particular, with a large number of azimuth channels, e.g., 24 channels in [153], the idea of Velocity SAR (VSAR) can be applied. Another novel idea is the introduction of sparse signal processing, where the moving targets are considered sparse signal and the objective is to separate moving target from stationary area targets. Simulation results showed that the velocity can be estimated with only two channels [155]. The second challenge lies in target detection with long SAT. Typical solutions include adaptive spatial filtering based on polynomial range model [137] and the application of neural networks [156], of which the latter can also reduce the computation burden significantly.

B. Systems with non-radar illuminator

To tackle the issues of insufficient observing timeliness caused by the limited number of spaceborne SAR missions,

heterogeneous distributed spaceborne SAR systems with non-radar illuminators are also essential. These illuminators primarily include communication satellites and navigation satellites. Such systems are also commonly called parasitic SAR [157]. Regarding communication satellites, they are divided into LEO, MEO, and GEO satellites. The heterogeneous distributed spaceborne SAR predominantly focuses on GEO communication satellites due to their larger signal bandwidth than LEO and MEO communication satellites. In 1998, researchers from POLIMI proposed the concept of GEO parasitic bistatic SAR [21], which uses a passive GEO satellite with a small eccentricity to form a synthetic aperture and reuse a Digital Audio Broadcast (DAB) satellite as the transmitter. It can achieve coarse imaging with a resolution of 120 m ~ 1 km and perform interferometry with a repeat time of 12 hours. Subsequently, they carried out the first demonstrative imaging experiment, but ground features were difficult to identify due to the low resolutions [158]. A recent communication satellite-based SS-BSAR experiment was carried out by researchers from University of Siegen in 2018, where a Digital Video Broadcasting (DVB) satellite, Intelsat 12, was employed as illuminator. They obtained the SAR image and repeat-pass interferogram of a 1.8 km × 3.2 km area, with an azimuth resolution of 1 m [159], as shown in Fig. 15, which again indicate the feasibility of communication satellite-based SS-BSAR. However, since broadcast satellites usually have near-geostationary orbits, the SAT is often very long (several hours), limiting application scenarios.

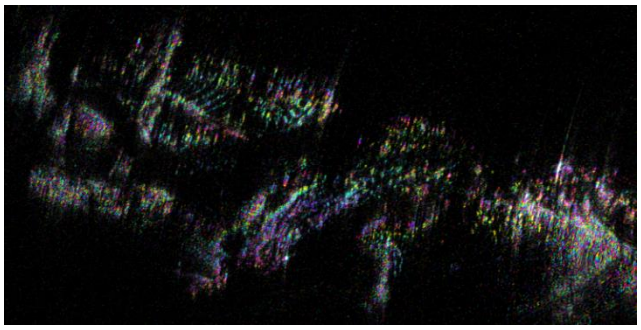

Fig. 15 DVB-based SS-BSAR experiment result. The intensity image of the scene overlaid with the interferometric phase [159].

In recent years, with the emergence of large-scale broadband communication satellites (such as Iridium, Starlink, and OneWeb [160, 161]), researchers have begun to explore the feasibility and performance of using these satellites as illuminators for passive radar or passive SAR imaging. Most recent works focus on the feasibility and performance of target detection. In 2019, researchers from University of Birmingham demonstrated that the ground Power Flux Density (PFD) of the Starlink is about -182 $\mathrm{dBW/m^2}$, which is 20 dB higher than that of GNSS-based illuminators [162]. In 2021, researchers from Warsaw University of Technology (WUT) collected Starlink signals to analyze their characteristics [163, 164]. Experiment results showed that under user demand, the transmission of Starlink can be composed of pulses with varying pulse spacing. Such signal is able to provide a bistatic range resolution of 1.25 m and a Doppler resolution of 750 Hz for one pulse on average. The frequency resolution can be improved through coherent accumulation of multiple pulses. In 2023, researchers from FHR demonstrated that the transmission signals are mainly pulsed when the satellite is in a lower elevation [165]. They also discussed the feasibility of broadband communication satellites for passive SAR imaging, and the result showed that an azimuth resolution better than 1 m can be achieved with a synthetic aperture time of 4 s.

However, the principal challenge in using broadband communication satellites for passive imaging lies in the significant contradiction between the communication signal waveform and radar imaging requirements. An example is that communication satellite signals are often continuous rather than pulsed, or pulsed signals are generally occasional, which is contradictory to the traditional bistatic SAR system. Shared waveforms [166, 167] for both communication and radar have not been applied in orbit, thus there are no reports of using broadband communication satellites for SAR imaging.

Different from communication satellites, GNSS signals are usually simple and can be considered as pulse signals with a duty cycle of 100% (usually the pulse length is 1 ms). At the same time, the pseudo-random codes of the GNSS have an ambiguity function like that of the LFM signal. Therefore, since firstly proposed by the researcher from University of Birmingham in 2002 [22], using GNSS signals for passive imaging was keeping popular research for more than 20 years, and most research focus on SS-BSAR. The first GNSS-based SS-BSAR image was obtained by researchers from University of Birmingham in 2006, with GLONASS as the illuminator [168]. Since then, they break through many key technologies such as synchronization methods based on direct wave, coherent change detection methods, and decorrelation models.

With the launch and maturity of Chinese navigation satellite system, Beidou, Chinese scholars have also carried out SS-BSAR research based on Beidou since 2012. A representative research team is from BIT, where their study covers Beidou-based SS-BSAR synchronization, imaging algorithms, deformation processing, etc [20]. They obtained the first Beidou-based SS-BSAR image in 2013 [126]. From 2015 to 2018, they conducted multiple Beidou-based SS-BSAR deformation measurement experiments and obtained millimeter-level 3-D deformation of strong man-made scatterers such as corner reflectors [125] and transponders [122]. Relevant results show that the most significant benefit of GNSS-based BSAR is that with multiple satellites, it can perform high-accuracy 3-D deformation retrieval continuously throughout the day and has great potential in geological disaster monitoring. Since 2022, they break through a series of key technologies for 3-D deformation measurement in GNSS-based BSAR system, covering optimal selection method of satellites [123], improved imaging algorithms [169], adaptive Permanent Scatterer (PS) points selection methods [170], multi-angle PS points association algorithms [171], and interferometric phase error compensation methods [172] etc. At present, miniaturized GNSS-based SS-BSAR deformation measurement equipment has been deployed over 100 locations in southwestern China, as shown in Fig. 16.

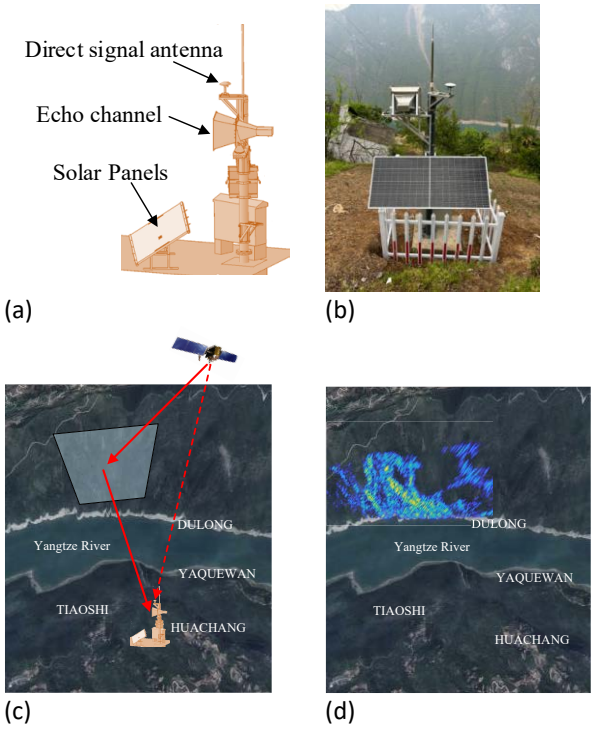

Fig. 16 Examples of deployed miniaturized Beidou-based SS-BSAR equipment for deformation measurement. (a) Beidou receiver model. (b) Beidou receiver prototype. (c) Observation geometry. (d) Example of SS-BSAR image.

Considering that communication satellites based SS-BSAR has not been completely verified, this article mainly reviews the key technologies of GNSS-based SS-BSAR, which mostly focus on 3-D deformation measurement recently, including combination of satellite, multi-angle PS association and phase error compensation [173].

To improve the performance of 3-D deformation measurement by GNSS-based SS-BSAR systems, an optimal GNSS satellite selection method was proposed [123]. The method is conducted under the criteria to maximize the number of PS points while constraining the resolution, theoretical 3-D deformation accuracy, and elevation angle of the utilized satellites within a reasonable range. The second challenge is the multi-angle PS points association methods, where the distributions of PS points between different GNSS-based SS-BSAR images are significant differences due to their diverse observation angles. To address it, an efficient association method was proposed, which uses the Intersection over Union (IOU) as the indicator to associate PS points [171]. To compensate phase errors in GNSS-based SS-BSAR interferograms is also one of the key technologies. Using a linear observation model considering residual height of the scene, and combined with optimal filtering algorithms, phase errors from DEM errors and atmospheric errors can be removed [172].

IV. Typical Applications of Distributed Spaceborne SAR

A. Image Enhancement

Thanks to the improved capability of SAR image acquisition by distributed spaceborne SARs, it becomes possible to perform image enhancement, such as ambiguity suppression [174, 175] and intensity enhancement, using multiple images. For homogenous spaceborne SAR, researchers from DLR conducted demonstrated experiments of Doppler ambiguity suppression using TerraSAR-X and TanDEM-X in 2014 [176]. They compared the single-channel SAR image acquired with a lower PRF than the nominal one, with the reconstructed image with two channels. The results were shown in Fig. 17. The quantitative analysis demonstrated a significant improvement in azimuth ambiguity-to-signal ratio (AASR) after ambiguity suppression.

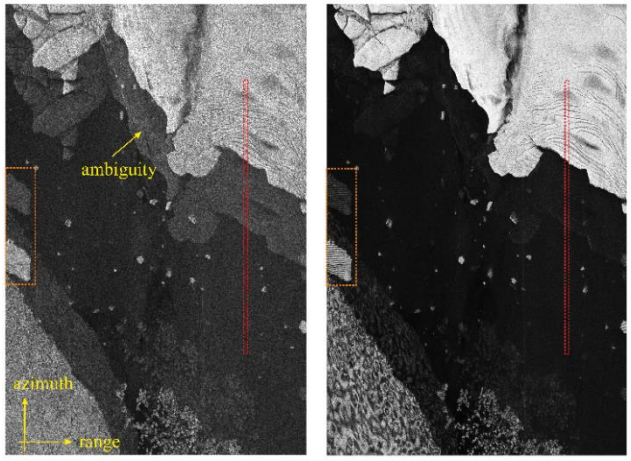

Fig. 17 Ambiguity suppression using TerraSAR-X and TanDEM-X [176]. (a) TerraSAR-X image shows strong azimuth ambiguities. (b) The reconstructed image based on the data of TerraSAR-X and TanDEM-X, where a much lower ambiguity level can be seen.

For heterogeneous distributed spaceborne SAR, researchers from BIT studied intensity enhancement methods of BeiDou-based SS-BSAR images based on image fusion in 2014. One method is to coherently fuse multiple repeat-pass images [177]. As shown in Fig. 18(a) and (b), by coherently fusing 22 images, the fused image has a much better contrast, with a SNR gain of 10.7 dB compared to a single image. The other is to enhance the intensity from multi-angle images. By fusing 26 SS-BiSAR images with significantly different view angles, the image details were greatly enhanced, and the SNR was improved [124, 126], as shown in Fig. 18(c) and (d). In 2015, researchers from Beihang University demonstrated that it is also feasible to enhance image resolution by jointly use Galileo E5 signals at different frequency points [178]. Recently, researchers from BIT proposed to improve the resolution of SS-BSAR image via spectrum synthesis, and the method was demonstrated by two repeat-pass Beidou-based images [179].

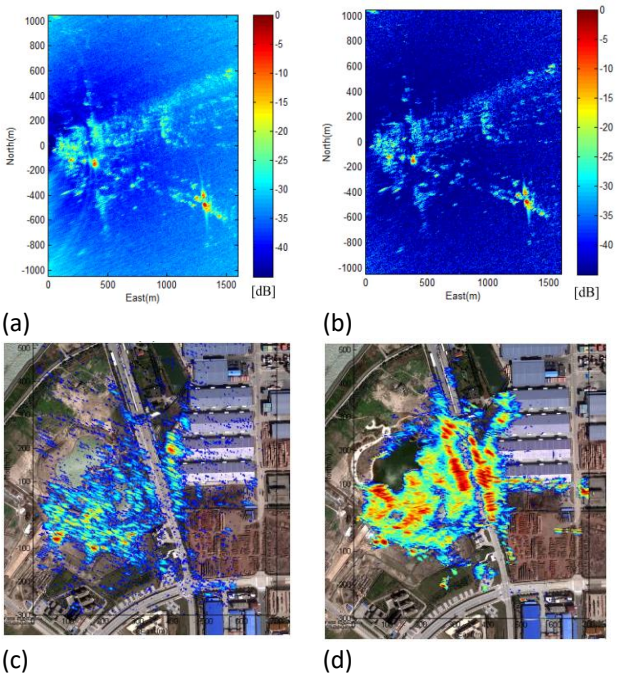

Fig. 18. Intensity enhancement of Beidou-based SS-BSAR images. (a) Incoherent fusion of 22 repeat-pass images. (b) Coherent fusion of 22 repeat-pass images [177]. (c) Single image. (d) Fused image from multi-angle images [124, 126].

There are also conceptual missions that are aimed at image enhancement. A typical example is the aforementioned ARGOS, which utilizes along-track formations to improve azimuth resolution [52]. For such formations, when the satellite trajectories are not completely coincident, grating lobes will occur due to discontinuous Doppler spectra. This can be resolved by optimizing SAT of each satellite [180].

Another popular application motivated by rich datasets of distributed spaceborne SAR is the Video SAR, which enables capabilities of dynamic scene monitoring [181]. In 2023, researchers from Capella used the Capella X-SAR to obtain 8 subaperture frames from a single-pass echo data of 30 second acquired in the spotlight mode. They used the open-source kernelized cross correlation (KCF) to track a moving vessel near harbors [182].

When utilizing bistatic/mulistatic and multi-angle images for image enhancement and fusion, it is necessary to pay special attention to two issues arising from geometric differences. The first is resolution degradation due to bistatic observation geometry [183], and the second is the scattering difference. The two issues raise challenges in fusion, which can be solved by intelligent solutions based on machine learning [184].

B. Terrain mapping

Terrain mapping is the most typical application of distributed spaceborne SAR, especially in close formation missions. The most typical system for DEM measurement in distributed spaceborne SAR is TanDEM-X. From 2010 to 2015, the TanDEM-X covered the entire continental Earth twice, and the first global TanDEM-X DEM was created and released in 2016 [185, 186]. The spatial resolution of the TanDEM-X DEM is 12 m at the equator, with an absolute vertical height accuracy better than 10 m. It is now one of the DEMs with the highest accuracy generated by spaceborne sensors. In 2017, the TanDEM-X mission decided to conduct an additional comprehensive coverage scan of the continental Earth, aiming to create an independent dataset between 2017 and 2020 to observe terrain changes. These data will contribute to the production of a new global DEM, TanDEM-X DEM 2020, scheduled for release in 2024 [186]. In addition to TanDEM-X, close formation missions such as TH-2, LT-1, Gaojing-2 and HT-1 have all acquired high-precision DEMs through single-pass methods, but they did not release global DEM products.

As the TanDEM-X mission has covered the globe multiple times, a new TanDEM-X DEM Change Map will be released based on the comparison between the upcoming TanDEM-X DEM 2020 and the first global DEM [187]. This will show the changes between the two global DEM data, reflecting variations in forest cover, glaciers, permafrost zones, and areas affected by human activities. In 2023, researchers from DLR obtained large-scale surface changes in several mining areas in Queensland, Australia, by comparing DEM changes. The results indicates that the rise and fall in some areas can approach or even exceed 30 m [187], as shown in Fig. 19. Some researchers also explored combining the TanDEM-X DEMs from ascending and descending orbits [188], and the results showed that the invisible areas can be reduced from 5.7% to 1.2% after fusion, but the accuracy is hardly improved.

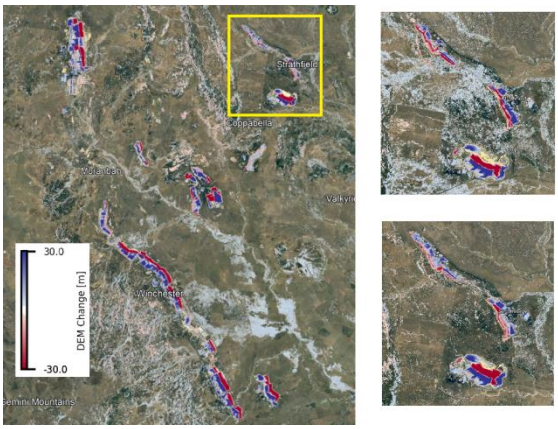

Fig. 19 TanDEM-X DEM Change Maps example over multiple coal mines in Queensland, Australia [187].

In addition to InSAR, another DEM generation method is radar photogrammetry, which requires multi-angle SAR images [189]. In 2023, researchers from the Centre Tecnològic de Telecomunicacions de Catalunya used two Capella X-SAR images, with resolutions of 0.7 m × 0.5 m and incident angles of 33° and 29.5°, to reconstruct the DEM of an approximately 7.2 km × 6 km area. The retrieved DEM has an accuracy of about 8.4 m [190], as shown in Fig. 20. With the rapid production of high-resolution images, this method has significant potential.

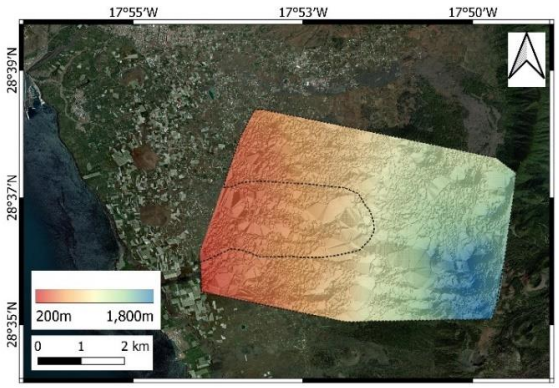

Fig. 20 Radargrammetry DEM using Capella X-SAR images [190].

For distributed spaceborne SAR with small scenes, especially for SS-BSAR, terrain mapping is primarily a way to verify the feasibility and capabilities of systems. Typical examples are the single-pass DEM inversion based on dual-antenna receiver conducted by researchers from UPC in 2008 [105, 106], BIT in 2012, and IECAS in 2013 [191, 192]. Another example is both the single-pass and repeat-pass DEM inversion by researchers from BIT, based on LT-1 in 2022 [130].

In addition to LEO distributed spaceborne SAR, researchers from BIT have also proposed the use of distributed GEO SAR for DEM measurement [56, 193]. The main advantage of distributed GEO SAR is high data rate due to its short repeat-pass time. A challenge faced by such system, especially for one working in a high band (e.g., Ka), is the non-stationary non-Gaussian phase error caused by the small-scale atmosphere and steep terrain. An effective solution to this problem is to introduce Particle Filter (PF), which can deal with non-Gaussian noise and improve the DEM measurement accuracy [193].

C. 3-D Imaging

3-D imaging has played a significant role in fields such as forest height measurement [194] and urban point cloud reconstruction [195, 196]. Currently, most research on 3-D imaging from distributed spaceborne SAR is based on TSX and TDX.

In 2013, researchers from DLR firstly used five dual-pol single-pass TSX/TDX interferograms with multiple baselines for forest observation and estimated the vertical structure of the forest [197]. With the Capon beamforming algorithm [198] applied, the height of canopy and bared soil can be estimated. In 2019, they referred to the single-pass interferogram-based tomography as coherence-based TomoSAR. Fourteen TSX/TDX interferograms were used to estimate the height of forest, where the complex coherence between repeat-pass image pairs were set to zero to suppress temporal decorrelation. The results showed that the coherence-based tomography has an accuracy of 2.7 m, which is much better than that of the classical Single-Look Complex (SLC) -based method (34.3 m) [194], as shown in Fig. 21.

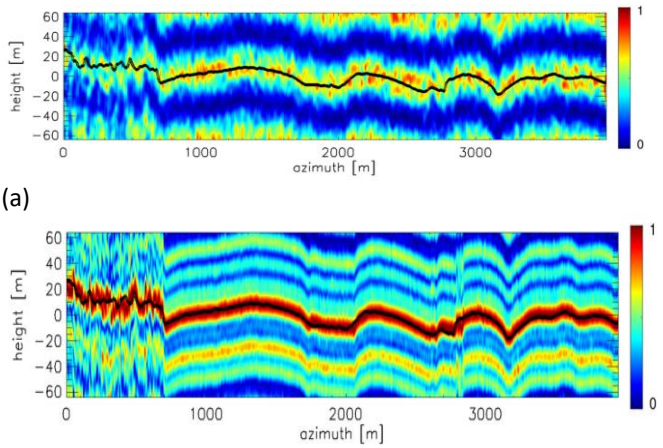

Fig. 21 Comparison between SLC-based and coherence-based tomography in the forest height retrieval. (a) Results of SLC-based tomography. (b) Coherence-based tomography [194].

The high-resolution images provided by TSX and TDX have driven the research in 3-D imaging for urban areas in recent years. It is demonstrated that fewer single-pass interferograms are required for urban 3-D imaging than for typical scenes using SLC SAR images, due to the high coherence in each single-pass interferometric pair. In 2020, researchers from DLR used 3 to 5 TSX/TDX interferograms to perform 3-D urban imaging. The results, as shown in Fig. 22, indicate that 62.8% of the buildings are reconstructed with an accuracy better than 2 m [195].

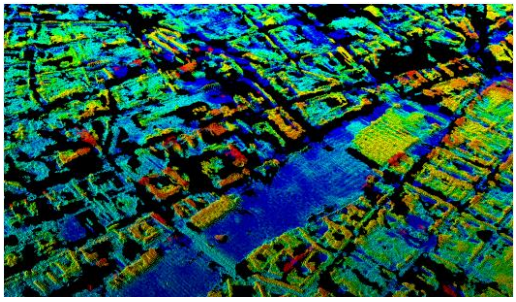

Fig. 22 Point clouds obtained by 3-D imaging in urban area [195]. 3~5 pairs of TSX/TDX images were used.

In heterogeneous distributed spaceborne SAR, the research on 3-D imaging is primarily focused on SS-BSAR, as it is much easier to collect multi-channel or repeat-pass data in SS-BSAR than SA-BSAR. Classical experiments include the transponder-based single-pass demonstration [108, 113, 129] and the repeat-pass tomography [131], both reviewed in Section III.

D. Deformation retrieval

The greatest advantage of distributed spaceborne SAR over a single-satellite SAR is the capability of providing multi-angle observations, enabling 3-D deformation measurement. This is an effective approach to address the issue of low deformation accuracy in the South-North direction of the traditional polar-orbiting SAR. Moreover, the timeliness of deformation measurement can also be improved via loose formations. Another notable advantage of distributed spaceborne SAR is

the scattering complementarity between monostatic and bistatic SAR, and between different observation angles, by which more PS points can be obtained by combining these acquisitions. The superiority has been demonstrated for PS points association in the GNSS-based SS-BSAR experiments for natural slope deformation measurements [171]. Particularly in urban areas, PS points are different between monostatic and bistatic SAR images. This diversity allows to integrate and increase the density of deformation measurement points [199], which is an important research direction in the future.

In terms of homogeneous distributed spaceborne SAR, both SESAME and Harmony have the capability of multi-angle observation. However, their multi-angle LOSs are nearly in the same plane, thus 3-D deformation should be measured through combining ascending and descending orbit acquisitions. In 2021, researchers from BIT proposed a three-satellite distributed GEO SAR system that can observe the scene from three angles simultaneously, which is able to retrieve centimeter-level 3-D deformation [17]. Tropospheric phase generally distorts deformation signals in D-InSAR processing. It is especially serious in the presence of tropospheric turbulence, which cannot be removed by using external numerical weather models. Regarding this, in 2023, they demonstrated that multi-angle distributed spaceborne SAR can retrieve multi-dimensional deformation and differential tropospheric delay (DTD) simultaneously to eliminate the impacts of tropospheric turbulence in deformation monitoring, where the results showed an accuracy of about 2 mm in 2-D deformation retrieval [200, 201], as shown in Fig. 23.

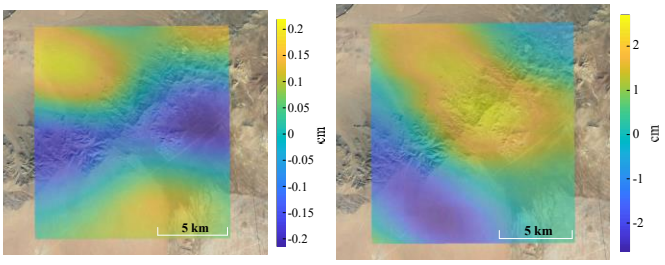

(a) (b)

Fig. 23 2-D deformation retrieved by the MWF method via multi-angle distributed SAR. (a) LOS deformation. (b) Azimuth deformation.

For heterogeneous distributed SAR, the primary research for deformation measurement is focused on GNSS-based SS-BSAR. In 2018, researchers from BIT demonstrated the capability of Beidou-based SS-BSAR to provide temporally continuous 3-D deformation measurement with millimeter-level accuracy [122]. Recently, with their proposed processing methods reviewed in Section III, 3-D deformation of area scene with millimeter-level accuracy was retrieved, as shown in Fig. 24. In 2023, they also explored the potential of retrieving 2-D deformation of SS-BSAR with LT-1 as the illuminator and two-angle receivers. The deformation has the accuracy of centimeter level, as shown in Fig. 25, indicating the potential of heterogeneous distributed SAR with radar-based illuminator in the aspect of multi-dimensional deformation measurements [130].

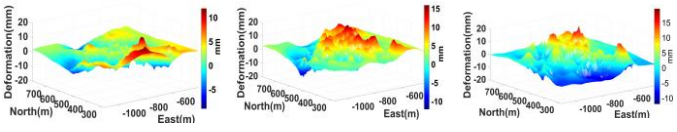

(a) (b) ©

Fig. 24 Retrieved 3-D deformation of Beidou-based SS-BSAR acquired by BIT. Deformation in the (a) East direction, (b) North direction, and (d) Zenith direction.

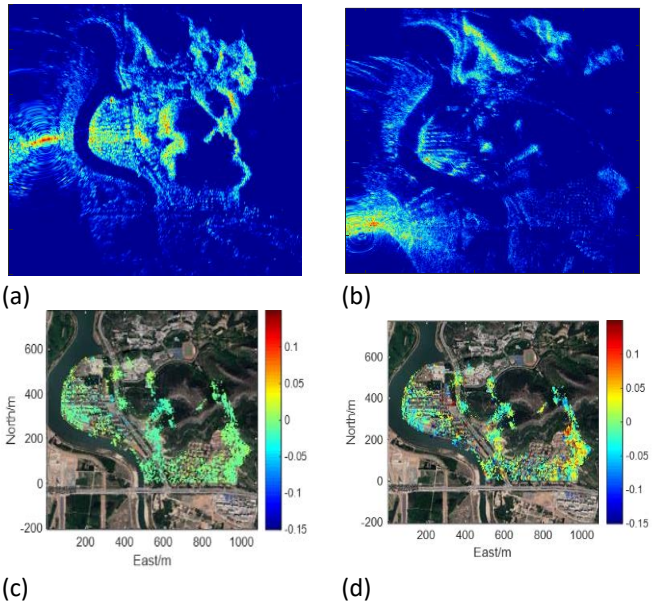

(a) (b)

(c) (d)

Fig. 25 Retrieved 2-D deformation of LT-1 -based SS-BSAR acquired by BIT. (a) SAR image of the first direction. (b) SAR image of the second direction. (c) The deformation in the equivalent LOS direction. (d) The deformation perpendicular to the equivalent LOS direction.

E. Atmosphere mapping

The spaceborne repeat-pass InSAR is inevitably affected by the temporally varying atmosphere, which researchers focus on removing when conducting deformation monitoring in general. Alternatively, in the absence of deformation, such as the data acquisition cases under very short InSAR repeat-pass period or over the stable ground surface, spaceborne D-InSAR can also be used to retrieve the LOS atmospheric parameters. However, a single satellite can only obtain the integrated atmospheric refractivity and water vapor along the LOS direction, unable to recover the 3-D atmospheric parameters, which limits the application scope of the related atmospheric products in meteorological monitoring and forecasting.

One configuration for 3-D atmospheric parameters retrieval is to use a multi-angle formation, with each multiple satellites' LOSs passing through the constructed 3-D atmospheric grids to realize atmospheric tomography processing. A representative research team in this field is the BIT. Since currently there are no in-orbit multi-angle formations, the research is mainly focused on theory and algorithms.

In 2017, researchers from BIT proposed that the 3-D ionospheric electron density can be tomographic retrieved by multiple L-band GEO SARs [202]. The main idea is firstly to

divide sub-bands in range and sub-apertures in azimuth and retrieve the Total Electron Content (TEC) along the LOS direction via spectrum splitting method. Then, the 3-D electron density can be reconstructed by solving equation set provided by observations from GEO SARs. Simulation results, as shown in Fig. 26(a), showed that with four GEO SARs, the ionospheric retrieval error is less than ±0.5 TECU, and the relative error is better than 1.5%. In 2021, researchers from TU Delft proposed the utilization of a C-band multi-angle formation to accurately estimate the zenith DTD in the presence of baseline knowledge errors. Taking the Harmony mission as an example, at least 300 km of inter-satellite distance is required for high-precision DTD estimation. The centimeter-level absolute accuracy and submillimeter-level relative accuracy of zenith DTD can be obtained by solving a mixed least-square (LS) problem [203]. Currently, researchers from BIT have been studying the retrieval method of 3-D differential tropospheric refractivity (DTR) using multi-angle formations. Simulation results, shown in Fig. 26(b), verified the feasibility of the method, with a millimeter-level accuracy of DTD with sub-kilometer resolution in the zenith direction [204].

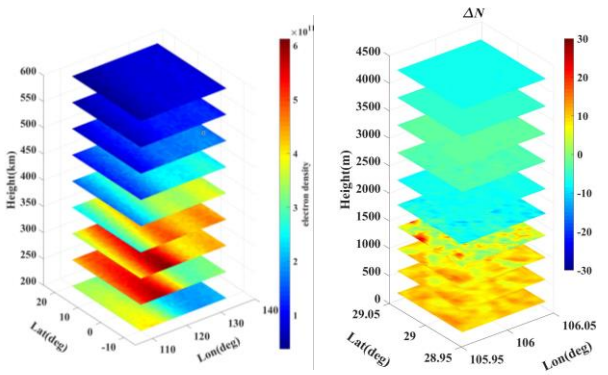

(a) (b)

Fig. 26 The simulated -3D atmospheric parameters retrieved by multi-angle formations. (a) The simulated recovered electron density. (b) The recovered DTR [204].

F. Ocean Observation

Similar to the 3-D deformation retrieval, multi-angle formations have significant capability for multi-dimensional parameter measurement over ocean surface, including 2-D ocean current field, ice drift measurement, etc [205]. A typical and dedicated distributed SAR system capable of conducting 2-D measurements of oceanic dynamic parameters is Harmony. Besides, employing special imaging mode such as bidirectional (BiDi) SAR mode [206], TanDEM-X also has such capability, which currently is also an effective mission to demonstrate the feasibility of Harmony. Typical processing methods are Doppler Centroid Anomaly (DCA) and ATI.

In terms of 2-D ocean current field measurement, researchers from TU Delft demonstrated that the additional LOS of Harmony with the stereo configuration can capture more components of the ocean wave spectrum, offering unique advantages in observing sea surfaces under high wind speed conditions such as tropical cyclone. Furthermore, it can enhance the observational features of the wave direction spectrum, helping the interpretation of bistatic, high-resolution sea surface scatter and Doppler measurements [207]. Under the stereo formation, Harmony is able to measure 2-D ocean current field with spatial resolutions ranging from 1 to 4 km and a sensitivity of about 15 cm/s [208].

In addition, researchers from BIT proposed a GEO-LEO bistatic SAR system with twin LEO receivers that can also provide 2-D ocean current measurements. The ATI phase model along with the distributed configuration optimization method in this system, are discussed in [209].

The measured data of distributed spaceborne SAR for ocean current measurements has far been implemented only in TanDEM-X. Researchers from TU Delft used the BiDi SAR mode data from TSX and TDX for ATI processing. With an azimuthal angular span of approximately 13.2° for the fore and aft beam, 2-D ocean current fields were acquired, which helps mapping and understanding sub-mesoscale (1-10 km) marine structures [206]. The aft look of data near Barents Sea and Kara Sea is shown in Fig. 27 (a), the resulting velocity error in fore and aft beam are 0.26 m/s and 0.55 m/s respectively [206]. Under hybrid baseline interferometry mode with both along-track and across-track baseline, Sea Surface Elevation (SSE) and principal wavelength of sea waves can be estimated, obtaining wave height with the error less than 0.1 m [210].

For sea ice drift measurement, it is analyzed by researchers from TU Delft that Harmony has the capability of measuring 3-D sea ice motion velocity vectors with high accuracy (< 100 mm/yr) and high resolution (better than 100 m × 100 m). As for the topography change (TOC) estimation for land ice, the mission can achieve an accuracy of 0.2 m/yr (goal). This will eventually contribute to the improvement of statistical and parameterized analysis of sea ice, helping for obtaining more accurate sea ice models [205]. What's more, the structure and deformation patterns of the sea ice can also be derived, which would be impossible with traditional methods such as feature tracking.

TanDEM-X is also indicated to be capable of measuring sea ice drift. All the typical modes of TanDEM-X, including bistatic single-pass InSAR, repeat-pass InSAR, and pursuit single-pass InSAR, are able to achieve diverse applications of sea ice monitoring as illustrated in Fig. 27 (b) [211]. Fig. 27 (c) shows an example of ice drift measured by TanDEM-X pursuit mode over the Chukchi Sea coast near Alaska. It can be seen that compared to landfast ice, the interferogram of pack ice exhibits a stronger phase response, i.e., largely cross-track parallel fringes, due to the faster motion of pack ice. The largely cross-track parallel fringes are likely a result from on-shore wind during the time of acquisition.

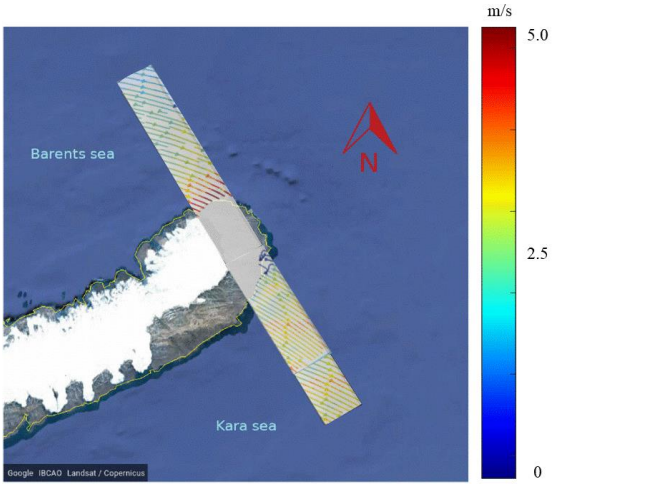

(a)

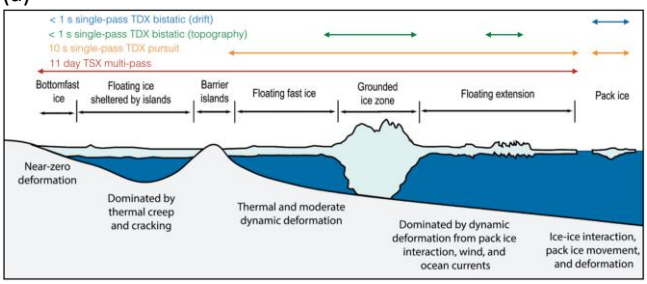

(b)

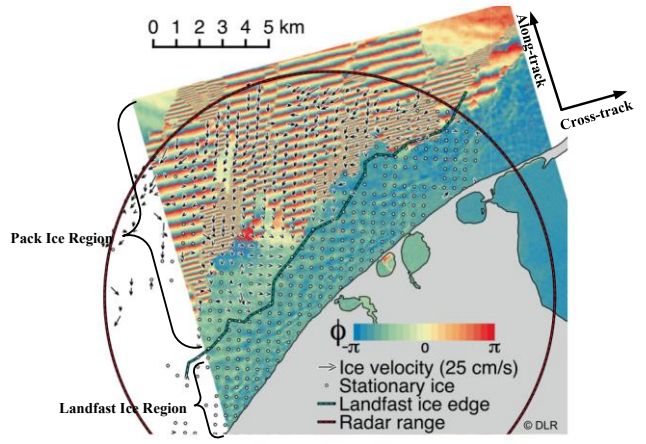

(c)

Fig. 27 Typical applications of ocean observation by TDX&TSX. (a) TDX&TSX Bidi SAR ATI acquisition over the Barents Sea and Kara Sea, revised from [210]. (b) Example of coastal sea ice and potential application of different TSX/TDX acquisition modes [211]. (c) TDX pursuit mode interferometric phase-derived motion over the Chukchi Sea coast near Alaska, revised from [211]. The arrows represent motion derived from ground-based radar data and land is masked out in gray.

V. Comments

Distributed spaceborne SAR has evolved over 30 years, observing significant progress made on both homogeneous and heterogeneous distributed spaceborne SAR. Various distributed systems which take SAR, navigation or communication satellites as illuminators have significant achievements in terms of system, signal processing, and application. Looking into the future, the primary development directions for distributed spaceborne SAR are anticipated to include:

In terms of the system, large-scale constellations will continue to evolve rapidly with increasing scale. This includes the multi-baseline large constellations characterized by close formation such as MirrorSAR and SwarmSAR, as well as large-scale loose constellations represented by Capella X-SAR and ICEYE. To achieve multi-dimensional parameter retrieval, multi-angle formations, such as Harmony, will continue to be developed and launched. With the scale expansion of satellite constellations, advanced multi-baseline multi-dimensional imaging [3-D, four-dimensional (4-D), and even five-dimensional (5-D) (3-D structure and 2-D deformation)], multi-angle terrestrial parameter inversion (2-D ocean currents, 3-D deformation, etc.), and hourly rapid response to the Earth's surface monitoring will become feasible. Spaceborne SAR will have a wider coverage range and shorter revisit/repeat time, enabling the acquisition of mass SAR data.

Thanks to the miniaturization and cost reduction of the receiving systems, the extensive deployment of spaceborne SAR and navigation satellites will provide an abundant source of illumination, facilitating the promotion and widespread adoption of heterogeneous distributed SAR based on large-scale satellites. Challenges in non-cooperative signal processing, and compensation of multi-source disturbance errors will be addressed in this kind of distributed SAR, which will promote their maturation in both technology and practical application.

On the other hand, with the continuous launch of thousands of broadband communication satellites, like Starlink and OneWeb, research on Integrated Radar and Communication System will get deepen. Considering the inherent contradictions between radar imaging and communication tasks, core issues such as waveform design and hardware compatibility will be gradually resolved. Experimental satellites accommodating both functionalities could be launched in the near future, and ultimately there will be in-orbit business satellites with relatively reliable detection and communication performance.

In terms of signal processing and application, the growing SAR data from distributed spaceborne SARs and the continuous improvement of Artificial Intelligence (AI) technology will facilitate the development of intelligent solutions significantly. AI will be applied more extensively not only in traditional SAR tasks for target interpretation and detection but also in multi-dimensional SAR imaging, InSAR/D-InSAR, etc. On-board real-time signal processing will also adopt intelligent methods. Additionally, the multiple radar nodes will promote the on-board processing to move towards a distributed and collaborative approach. For applications, the use of AI in the distributed spaceborne SAR data processing will become more widespread. The potential applications will not be limited to the traditional tasks of target detection, recognition and classification, but even the tasks of decision-making and prediction in disaster monitoring and prevention.

With increasingly accessible resources for large-scale AI models, signal processing and applications in distributed

spaceborne SARs will also benefit from it, but simultaneously, challenges of computational burden and power requirements will also arise. Although conventional methods (especially those derived from exact analytical models, e.g., 2-D imaging algorithms) possess good robustness, after the introduction of AI, many methods will be effectively improved in their computational speeds and resources consumption within an acceptable performance loss. Therefore, in the era of AI, discerning performance boundaries and exploring the degree of integration with AI in distributed spaceborne SARs will also remain a persistent topic of interest.

ACKNOWLEDGMENT

This work was supported in part by the National Natural Science Foundation of China under Grant 61960206009, Grant 62101039, Grant 62201051, and Grant 62471042; in part by the Shandong Excellent Young Scientists Fund Program (Overseas).

REFERENCES

[1] J. C. Curlander and R. N. Mcdonough, *Synthetic Aperture Radar: Systems and Signal Processing* (Wiley). New York: Wiley, 1991.

[2] K. Tomiyasu, "Tutorial review of synthetic-aperture radar (SAR) with applications to imaging of the ocean surface," *Proceedings of the IEEE,* vol. 66, no. 5, pp. 563-583, 1978, doi: 10.1109/proc.1978.10961.

[3] A. Moreira, P. Prats-Iraola, M. Younis, G. Krieger, I. Hajnsek, and K. P. Papathanassiou, "A tutorial on synthetic aperture radar," *IEEE Geoscience and Remote Sensing Magazine,* vol. 1, no. 1, pp. 6-43, 2013, doi: 10.1109/mgrs.2013.2248301.

[4] J. P. Laboratory. "NISAR Mission Concept." https://nisar.jpl.nasa.gov/mission/mission-concept/ (accessed.

[5] X. Dong, Y. Sui, Y. Li, Z. Chen, and C. Hu, "Repeat Ground Track SAR Constellation Design Using Revisit Time Image Extrapolation and Lookup-Table-Based Optimization," *IEEE Transactions on Geoscience and Remote Sensing,* vol. 61, pp. 1-13, 2023, doi: 10.1109/tgrs.2023.3304663.

[6] F. Caltagirone, A. Coletta, and G. De Luca, "COSMO-SkyMed mission and products description," *Italian Space Agency Doc.,* 2016.

[7] R. Hanssen, *Radar Interferometry* (Remote Sensing and Digital Image Processing). KLUWER ACADEMIC PUBLISHERS, 2001.

[8] R. J. Michaelides, H. A. Zebker, and Y. Zheng, "An Algorithm for Estimating and Correcting Decorrelation Phase From InSAR Data Using Closure Phase Triplets," *IEEE Transactions on Geoscience and Remote Sensing,* vol. 57, no. 12, pp. 10390-10397, 2019, doi: 10.1109/tgrs.2019.2934362.

[9] Y. Ji *et al.*, "Equatorial Ionospheric Scintillation Measurement in Advanced Land Observing Satellite (ALOS) Phased Array-Type L-Band Synthetic Aperture Radar (PALSAR) Observations," *Engineering,* 2024/03/24/ 2024, doi: 10.1016/j.eng.2024.01.027.

[10] G. Krieger, I. Hajnsek, K. P. Papathanassiou, M. Younis, and A. Moreira, "Interferometric Synthetic Aperture Radar (SAR) Missions Employing Formation Flying," *Proceedings of the IEEE,* vol. 98, no. 5, pp. 816-843, 2010, doi: 10.1109/jproc.2009.2038948.

[11] G. Krieger *et al.*, "TanDEM-X: A Satellite Formation for High-Resolution SAR Interferometry," *IEEE Transactions on Geoscience and Remote Sensing,* vol. 45, no. 11, pp. 3317-3341, 2007, doi: 10.1109/tgrs.2007.900693.

[12] P. López-Dekker *et al.*, "Companion SAR constellations for single-pass interferometric applications: The SESAME mission," in *2017 IEEE International Geoscience and Remote Sensing Symposium (IGARSS)*, 23-28 July 2017 2017, pp. 119-122, doi: 10.1109/IGARSS.2017.8126908.

[13] P. López-Dekker *et al.*, "The Harmony Mission: End of Phase-0 Science Overview," in *2021 IEEE International Geoscience and Remote Sensing Symposium IGARSS*, 11-16 July 2021 2021, pp. 7752-7755, doi: 10.1109/IGARSS47720.2021.9554896.

[14] T. Long, C. Hu, Z. Ding, X. Dong, W. Tian, and T. Zeng, *Geosynchronous SAR: System and Signal Processing*. Springer, 2018.

[15] J. NASA, "Global Earthquake Satellite System: a 20-year plan to enable earthquake prediction," 2003.

[16] A. Monti Guarnieri, A. Broquetas, A. Recchia, F. Rocca, and J. Ruiz-Rodon, "Advanced Radar Geosynchronous Observation System: ARGOS," *IEEE Geoscience and Remote Sensing Letters,* vol. 12, no. 7, pp. 1406-1410, 2015, doi: 10.1109/lgrs.2015.2404214.

[17] Y. Xie, Z. Chen, Y. Li, X. Dong, and C. Hu, "Three-Dimensional Deformation Retrieval by Multi-Angle Processing in Distributed Geosynchronous SAR," in *2021 CIE International Conference on Radar (Radar)*, 15-19 Dec. 2021 2021, pp. 531-534, doi: 10.1109/Radar53847.2021.10028116.

[18] H. Zhang *et al.*, "Spaceborne/Stationary Bistatic SAR Imaging With TerraSAR-X as an Illuminator in Staring-Spotlight Mode," *IEEE Transactions on Geoscience and Remote Sensing,* vol. 54, no. 9, pp. 5203-5216, 2016, doi: 10.1109/tgrs.2016.2558294.

[19] Z. Sun *et al.*, "Spaceborne-Airborne Bistatic SAR Experiment Using GF-3 Illuminator: Description, Processing and Results," in *2021 IEEE International Geoscience and Remote Sensing Symposium IGARSS*, 11-16 July 2021 2021, pp. 2699-2702, doi: 10.1109/IGARSS47720.2021.9554025.

[20] Y. Zhang, Y. Li, Z. Chen, X. Zhao, Y. Liu, and C. Hu, "First Result of Lutan-1 Space-Surface Bistatic SAR Interferometry," in *IGARSS 2023 - 2023 IEEE International Geoscience and Remote Sensing Symposium*, 16-21 July 2023 2023, pp. 7860-7863, doi: 10.1109/IGARSS52108.2023.10282986.

[21] C. Prati, F. Rocca, D. Giancola, and A. M. Guarnieri, "Passive geosynchronous SAR system reusing backscattered digital audio broadcasting signals," *IEEE Transactions on Geoscience and Remote Sensing,* vol. 36, no. 6, pp. 1973-1976, 1998, doi: 10.1109/36.729370.

[22] M. Cherniakov, "Space-surface bistatic synthetic aperture radar - prospective and problems," in *RADAR 2002*, 15-17 Oct. 2002 2002, pp. 22-25, doi: 10.1109/RADAR.2002.1174646.

[23] H. Taud and J.-F. J. G. r. Parrot, processus, environnement, "Measurement of DEM roughness using the local fractal dimension," vol. 11, no. 4, pp. 327-338, 2005.

[24] M. Seidel, P. Marzahn, and R. Ludwig, "Monitoring of a Sea-Dike in Northern Germany by Means of ERS-1, ENVISAT/ASAR, and Sentinel-1 SAR Interferometry," *IEEE Journal of Selected Topics in Applied Earth Observations and Remote Sensing,* vol. 12, no. 11, pp. 4351-4360, 2019, doi: 10.1109/jstars.2019.2949244.

[25] D. Massonnet, "Capabilities and limitations of the interferometric cartwheel," *IEEE Transactions on Geoscience and Remote Sensing,* vol. 39, no. 3, pp. 506-520, 2001, doi: 10.1109/36.911109.

[26] J. G. Ender, "Spacebased SAR/MTI using multistatic satellite configurations," in *4th European Conference on Synthetic Aperture Radar (EUSAR 2002)*, 2002.

[27] L. Iannini, O. Dogan, P. Hoogeboom, and P. Lopez-Dekker, "Dimension-Adaptive Imaging with a SwarmSAR of Lightweight S-Band Nodes," in *2021 IEEE International Geoscience and Remote Sensing Symposium IGARSS*, 11-16 July 2021 2021, pp. 1098-1101, doi: 10.1109/IGARSS47720.2021.9553428.

[28] J. Mittermayer *et al.*, "MirrorSAR: An HRWS Add-On for Single-Pass Multi-Baseline SAR Interferometry," *IEEE Transactions on Geoscience and Remote Sensing,* vol. 60, pp. 1-18, 2022, doi: 10.1109/tgrs.2021.3132384.

[29] Z. Chen, C. Hu, X. Dong, Y. Li, W. Tian, and S. Hobbs, "Coherence-Based Geosynchronous SAR Tomography Employing Formation Flying: System Design and Performance Analysis," *IEEE Transactions on Geoscience and Remote Sensing,* vol. 59, no. 9, pp. 7165-7179, 2021, doi: 10.1109/tgrs.2021.3056209.

[30] Y. Li *et al.*, "A Novel PF-Based Method for Height Reconstruction in Distributed Geosynchronous Repeat-Pass InSAR," *IEEE Transactions on Geoscience and Remote Sensing,* vol. 61, pp. 1-15, 2023, doi: 10.1109/tgrs.2023.3308171.

[31] A. Moreira *et al.*, "TanDEM-X: a TerraSAR-X add-on satellite for single-pass SAR interferometry," in *IGARSS 2004. 2004 IEEE International Geoscience and Remote Sensing Symposium*, 20-24 Sept. 2004 2004, vol. 2, pp. 1000-1003 vol.2, doi: 10.1109/IGARSS.2004.1368578.

[32] S. Buckreuss and M. Zink, "TerraSAR-X and TanDEM-X Mission Status," in *Proceedings of EUSAR 2016: 11th European Conference on Synthetic Aperture Radar*, 6-9 June 2016 2016, pp. 1-6.

[33] S. V. Baumgartner *et al.*, "Bistatic experiment using TerraSAR-X and DLR's new F-SAR system," in *7th European Conference on Synthetic Aperture Radar, EUSAR 2008, June 2, 2008 - June 5, 2008*, Friedrichshafen, Germany, 2008, vol. 1-4: Institute of Electrical and Electronics Engineers Inc., in Proceedings of the European Conference on Synthetic Aperture Radar, EUSAR.

[34] I. Walterscheid *et al.*, "Bistatic SAR Experiments With PAMIR and TerraSAR-X—Setup, Processing, and Image Results," *IEEE Transactions on Geoscience and Remote Sensing,* vol. 48, no. 8, pp. 3268-3279, 2010, doi: 10.1109/tgrs.2010.2043952.
[35] Z. L. L. Lou, H. Zhang, F. Qian, and X. Zhang, "Key technologies of TH-2 satellite system," *Acta Geodaetica et Cartographica Sinica,* vol. 51, no. 12, pp. 2403-2416, 2022, doi: 10.11947/j.AGCS.2022.20210567.
[36] Z. L. L. Lou, H. Zhang, F. Qian, and Y. Huang, "TH-2 satellite engineering design and implementation," *Acta Geodaetica et Cartographica Sinica,* vol. 49, no. 10, pp. 1252-1264, 2020, doi: 10.11947/j.AGCS.2020.20200175.
[37] X. T. T. Li, S. Li, X. Zhou, X. Zhang, and Y. Xu, "Classification of basic deformation products of L-band differential interfero-metric SAR satellite," *Acta Geodaetica et Cartographica Sinica,* vol. 52, no. 5, pp. 769-779, 2023, doi: 10.11947/j.AGCS.2023.20220050.
[38] X. Zhang, X. Tang, T. Li, H. Zhao, X. Zhang, and L. Li, "Coherence Analysis of Lutan-1 Satellite with Two Formations for Different Scenes," in *2023 SAR in Big Data Era (BIGSARDATA)*, 20-22 Sept. 2023 2023, pp. 1-4, doi: 10.1109/BIGSARDATA59007.2023.10294880.
[39] Y. Ji *et al.*, "Mining Deformation Monitoring Based on Lutan-1 Monostatic and Bistatic Data," *Remote Sensing,* vol. 15, no. 24, p. 5668, 2023, doi: 10.3390/rs15245668.
[40] W. Y. Y. Deng, H. Zhang, W. Wang, D. Liu, and R. Wang, "Forthcoming Spaceborne SAR Development," *Journal of Radars,* vol. 9, no. 1, p. 1, 2020-02-28 2020, doi: 10.12000/jr20008.
[41] G. Jin *et al.*, "Nonlinear Frequency Modulation Signal Generator in LT-1," *IEEE Geoscience and Remote Sensing Letters,* vol. 16, no. 10, pp. 1570-1574, 2019, doi: 10.1109/lgrs.2019.2905359.
[42] R. Torres, S. Lokas, H. L. Moller, M. Zink, and D. M. Simpson, "The TerraSAR-L mission and system," in *IGARSS 2004. 2004 IEEE International Geoscience and Remote Sensing Symposium*, 20-24 Sept. 2004 2004, vol. 7, pp. 4519-4522 vol.7, doi: 10.1109/IGARSS.2004.1370159.
[43] D. B. Tridon *et al.*, "Tandem-L observation concept - contributions and challenges of systematic monitoring of earth system dynamics," in *2017 18th International Radar Symposium (IRS)*, 28-30 June 2017 2017, pp. 1-9, doi: 10.23919/IRS.2017.8008159.
[44] G. Krieger *et al.*, "The tandem-L mission proposal: Monitoring earth's dynamics with high resolution SAR interferometry," in *2009 IEEE Radar Conference*, 4-8 May 2009 2009, pp. 1-6, doi: 10.1109/RADAR.2009.4977077.
[45] G. Krieger *et al.*, "MirrorSAR: A fractionated space radar for bistatic, multistatic and high-resolution wide-swath SAR imaging," in *2017 IEEE International Geoscience and Remote Sensing Symposium (IGARSS)*, 23-28 July 2017 2017, pp. 149-152, doi: 10.1109/IGARSS.2017.8126916.
[46] J. Mittermayer, G. Krieger, and A. Moreira, "Concepts and Applications of Multi-static MirrorSAR Systems," in *2020 IEEE Radar Conference (RadarConf20)*, 21-25 Sept. 2020 2020, pp. 1-6, doi: 10.1109/RadarConf2043947.2020.9266479.
[47] L. Iannini, P. Lopez-Dekker, and P. Hoogeboom, "A Highly Flexible and Scalable S-band SwarmSAR from Very Simple Nodes," in *2020 IEEE Radar Conference (RadarConf20)*, 21-25 Sept. 2020 2020, pp. 1-6, doi: 10.1109/RadarConf2043947.2020.9266527.
[48] M. G. Rodriguez, J. M. C. Muñoz, E. M. V. Carrasco, and N. A. Llorente, "Precursor - ECO: Inta Sar Mission Based on Collaborative Small Satellites," in *IGARSS 2023 - 2023 IEEE International Geoscience and Remote Sensing Symposium*, 16-21 July 2023 2023, pp. 1521-1524, doi: 10.1109/IGARSS52108.2023.10282313.
[49] J. Ruiz Rodon, A. Broquetas, A. Monti Guarnieri, and F. Rocca, "Geosynchronous SAR Focusing With Atmospheric Phase Screen Retrieval and Compensation," *IEEE Transactions on Geoscience and Remote Sensing,* vol. 51, no. 8, pp. 4397-4404, 2013, doi: 10.1109/tgrs.2013.2242202.
[50] C. Hu, T. Long, T. Zeng, F. Liu, and Z. Liu, "The Accurate Focusing and Resolution Analysis Method in Geosynchronous SAR," *IEEE Transactions on Geoscience and Remote Sensing,* vol. 49, no. 10, pp. 3548-3563, 2011, doi: 10.1109/tgrs.2011.2160402.
[51] A. M. Guarnieri, S. Tebaldini, F. Rocca, and A. Broquetas, "GEMINI: Geosynchronous SAR for Earth Monitoring by Interferometry and Imaging," in *2012 IEEE International Geoscience and Remote Sensing Symposium*, 22-27 July 2012 2012, pp. 210-213, doi: 10.1109/IGARSS.2012.6351601.
[52] A. M. Guarnieri *et al.*, "ARGOS: A fractioned geosynchronous SAR," *Acta Astronautica,* vol. 164, pp. 444-457, 2019, doi: 10.1016/j.actaastro.2015.11.022.
[53] T. Y. Erkeç and C. Hajiyev, "Relative State Estimation for Two-Satellite Formation with Three Extented Kalman Filters Architecture using GNSS Receivers," in *2023 10th International Conference on Recent Advances in Air and Space Technologies (RAST)*, 7-9 June 2023 2023, pp. 1-6, doi: 10.1109/RAST57548.2023.10197966.
[54] G. Krieger, "Advanced Bistatic and Multistatic SAR Concepts and Applications," in *European Conference on Synthetic Aperture Radar*, 2006, pp. 1-101.
[55] E. C. D. Grandi, E. T. A. Mitchard, I. H. Woodhouse, A. Verhegghen, and F. Muirhead, "Statistics of TanDEM-X DSM, coherence and backscatter for the characterization of tropical forest structural configuration," in *2015 IEEE International Geoscience and Remote Sensing Symposium (IGARSS)*, 26-31 July 2015 2015, pp. 1805-1808, doi: 10.1109/IGARSS.2015.7326141.
[56] Z. Chen, X. Dong, Y. Li, and C. Hu, "Formation Design for Single-Pass GEO InSAR Considering Earth Rotation Based on Coordinate Rotational Transformation," *Remote Sensing,* vol. 12, no. 3, p. 573, 2020.
[57] Z. Chen, Y. Li, C. Li, Y. Liu, X. Dong, and C. Hu, "Analysis of General Geometric Decorrelation in Interferometric SAR," *IEEE Geoscience and Remote Sensing Letters,* vol. 19, pp. 1-5, 2022, doi: 10.1109/lgrs.2022.3187070.
[58] C. Hu, Y. Li, X. Dong, and T. Long, "Optimal data acquisition and height retrieval in repeat-track geosynchronous SAR interferometry," *Remote Sensing,* vol. 7, no. 10, pp. 13367-13389, 2015.
[59] J. Y. e. al, "A Review on Development of Formation Flying Interferometric SAR Satellite System," *Spacecraft Engineering,* no. 1, pp. 116-122, 2018.
[60] G. Jin *et al.*, "An Advanced Phase Synchronization Scheme for LT-1," *IEEE Transactions on Geoscience and Remote Sensing,* vol. 58, no. 3, pp. 1735-1746, 2020, doi: 10.1109/tgrs.2019.2948219.
[61] O. Montenbruck, L. V. Barneveld, Y. Yoon, and P. Visser, "GPS-Based Precision Baseline Reconstruction for the TanDEM-X SAR-Formation," in *20th International Symposium on Space Flight Dynamics*, 2007.
[62] M. Rothacher *et al.*, "The Tracking, Occultation and Ranging (TOR) instrument onboard TerraSAR-X and on TanDEM-X," in *2007 IEEE International Geoscience and Remote Sensing Symposium*, 23-28 July 2007 2007, pp. 4983-4986, doi: 10.1109/IGARSS.2007.4423980.
[63] K. Scipal and M. Davidson, "The SAOCOM-CS mission: ESA's first bistatic and tomographic L-band mission," in *2017 IEEE International Geoscience and Remote Sensing Symposium (IGARSS)*, 23-28 July 2017 2017, pp. 123-124, doi: 10.1109/IGARSS.2017.8126909.
[64] Y. Li, P. Lopez-Dekker, L. Iannini, and P. Prats-Iraola, "Performance of 2-D Deformation Measurements by the Multi-Static Harmony (Stereoid) Mission," in *IGARSS 2019 - 2019 IEEE International Geoscience and Remote Sensing Symposium*, 28 July-2 Aug. 2019 2019, pp. 8826-8829, doi: 10.1109/IGARSS.2019.8900151.
[65] ESA, "Report for Mission Selection: Earth Explorer 10 Candidate Mission Harmony," European Space Agency, Noordwijk, The Netherlands, ESA-EOPSM-HARM-RP-4129, 2022.
[66] G. D. Krebs. "Harmony A, B (Earth Explorer 10)." Gunter's Space Page. https://space.skyrocket.de/doc_sdat/harmony.htm (accessed.
[67] ESA. "ESA selects Harmony as tenth Earth Explorer mission." (accessed 22 September.
[68] P. Lopez Dekker, H. Rott, B. Chapron, and P. Prats-Iraola, Stereo Thermo-Optically Enhanced Radar for Earth, Ocean, Ice, and land Dynamics (STEREOID). 2018.
[69] P. López-Dekker, Y. Li, L. Iannini, P. Prats-Iraola, and M. Rodríguez-Cassola, "On Azimuth Ambiguities Suppression for Short-Baseline Along-Track Interferometry: the Stereoid Case," in *IGARSS 2019 - 2019 IEEE International Geoscience and Remote Sensing Symposium*, 28 July-2 Aug. 2019 2019, pp. 110-113, doi: 10.1109/IGARSS.2019.8898126.
[70] P. Lopez Dekker et al., The Harmony Mission: End of Phase-0 Science Overview. 2021, pp. 7752-7755.
[71] A. Theodosiou and P. López-Dekker, "On the Sensitivity to Height and Motion of Bistatic SAR Interferometry: A Spectral View," *IEEE Transactions on Geoscience and Remote Sensing,* vol. 62, pp. 1-12, 2024, doi: 10.1109/tgrs.2024.3399598.
[72] P. Prats-Iraola *et al.*, "Role of the Orbital Tube in Interferometric Spaceborne SAR Missions," *IEEE Geoscience and Remote Sensing Letters,* vol. 12, no. 7, pp. 1486-1490, 2015, doi: 10.1109/lgrs.2015.2409885.
[73] A. J. A. Kolovos, S. Management, and C. Laboratory, "Persian Gulf War: The First Space War. A Critical Assessment of Space Systems," 2017.
[74] R. A. McDonald *et al.*, "National Reconnaissance Almanac," ed: NATIONAL RECONNAISSANCE OFFICE CHANTILLY VA, 2011.

[75] A. Anghel, R. Cacoveanu, A.-S. Moldovan, B. Rommen, and M. Datcu, "COBIS: Opportunistic C-Band Bistatic SAR Differential Interferometry," *IEEE Journal of Selected Topics in Applied Earth Observations and Remote Sensing,* vol. 12, no. 10, pp. 3980-3998, 2019, doi: 10.1109/jstars.2019.2939194.
[76] ESA. "Satellite Constellation." https://www.esa.int/Our_Activities/Observing_the_Earth/Copernicus/Sentinel-1/Satellite_constellation (accessed.
[77] G. Kroupnik, D. D. Lisle, S. Côté, M. Lapointe, C. Casgrain, and R. Fortier, "RADARSAT Constellation Mission Overview and Status," in *2021 IEEE Radar Conference (RadarConf21)*, 7-14 May 2021 2021, pp. 1-5, doi: 10.1109/RadarConf2147009.2021.9455298.
[78] L. Zhao *et al.*, "China's Gaofen-3 Satellite System and Its Application and Prospect," *IEEE Journal of Selected Topics in Applied Earth Observations and Remote Sensing,* vol. 14, pp. 11019-11028, 2021, doi: 10.1109/jstars.2021.3122304.
[79] J.-P. J. A. Sanfourche and S. Europe, "'SAR-lupe', an important German initiative," vol. 2, no. 4, pp. 26-27, 2000, doi: 10.1016/S1290-0958(01)80008-3
[80] J. A. Euillades *et al.*, "Interferometric Assessment of SAOCOM-1 TOPSAR Data," *IEEE Geoscience and Remote Sensing Letters,* vol. 21, pp. 1-5, 2024, doi: 10.1109/lgrs.2023.3347030.
[81] F. Covello *et al.*, "COSMO-SkyMed an existing opportunity for observing the Earth," vol. 49, no. 3-4, pp. 171-180, 2010.
[82] D. Castelletti *et al.*, "Capella Space VHR SAR Constellation: Advanced Tasking Patterns and Future Capabilities," in *IGARSS 2022 - 2022 IEEE International Geoscience and Remote Sensing Symposium*, 17-22 July 2022 2022, pp. 4137-4140, doi: 10.1109/IGARSS46834.2022.9884458.
[83] V. Ignatenko, P. Laurila, A. Radius, L. Lamentowski, O. Antropov, and D. Muff, "ICEYE Microsatellite SAR Constellation Status Update: Evaluation of first commercial imaging modes," in *IGARSS 2020-2020 IEEE International Geoscience and Remote Sensing Symposium*, 2020: IEEE, pp. 3581-3584.
[84] T. Obata, M. Arai, S. Asada, T. Imaizumi, H. Saito, and S. Shirasaka, "The Latest Status of Our Commercial Small Synthetic Aperture Radar Satellite Constellation," in *IGARSS 2020 - 2020 IEEE International Geoscience and Remote Sensing Symposium*, 26 Sept.-2 Oct. 2020 2020, pp. 3578-3580, doi: 10.1109/IGARSS39084.2020.9323284.
[85] spacenews. "Chinese partnership to create Tianxian SAR satellite constellation." https://spacenews.com/chinese-partnership-to-create-tianxian-sar-satellite-constellation/ (accessed.
[86] "Haisi 1 - Gunter's Space Page.Available: https://space.skyrocket.de/doc_sdat/haisi-1.htm." (accessed.
[87] "Qilu 1 - Gunter's Space Page.Available: https://space.skyrocket.de/doc_sdat/qilu-1.htm." (accessed.
[88] "New SAR satellite launched, with improved capabilities.Available:https://en.spacety.com/index.php/2022/03/01/two-new-satellites-launched-including-the-2nd-sar-satellite-with-improved-capabilities." (accessed.
[89] S. Zhang, F. Liu, Z. Wang, C. Wang, R. Lv, and D. Yao, "A LEO Spaceborne-Airborne Bistatic SAR Imaging Experiment," in *2022 IEEE International Conference on Signal Processing, Communications and Computing (ICSPCC)*, 25-27 Oct. 2022 2022, pp. 1-5, doi: 10.1109/ICSPCC55723.2022.9984341.
[90] M. Cherniakov, "Space-surface bistatic synthetic aperture radar-prospective and problems," pp. 22-25, 2002, doi: 10.1049/cp：20020241.
[91] T. Zeng, F. Liu, C. Hu, and T. Long, "Image Formation Algorithm for Asymmetric Bistatic SAR Systems With a Fixed Receiver," *IEEE Transactions on Geoscience and Remote Sensing,* vol. 50, no. 11, pp. 4684-4698, 2012, doi: 10.1109/tgrs.2012.2190937.
[92] A. Anghel, R. Cacoveanu, A. S. Moldovan, C. Savlovschi, B. Rommen, and M. Datcu, "Bistatic SAR imaging with Sentinel-1 operating in TOPSAR mode," in *2017 IEEE Radar Conference (RadarConf)*, 8-12 May 2017 2017, pp. 0601-0605, doi: 10.1109/RADAR.2017.7944274.
[93] A. Anghel, R. Cacoveanu, A. Popescu, and A. Moldovan, "Dual-band Bistatic SAR system with satellite emitter of opportunity and ground-based receiver," in *2016 International Conference on Communications (COMM)*, 2016: IEEE, pp. 473-476, doi: 10.1109/ICComm.2016.7528268.
[94] J. Sanz-Marcos, P. Lopez-Dekker, J. J. Mallorqui, A. Aguasca, and P. Prats, "SABRINA: A SAR Bistatic Receiver for Interferometric Applications," *IEEE Geoscience and Remote Sensing Letters,* vol. 4, no. 2, pp. 307-311, 2007, doi: 10.1109/lgrs.2007.894144.
[95] J. Sanz-Marcos, J. Mallorqui, A. Aguasca, and P. Prats, "First ENVISAT and ERS-2 Parasitic Bistatic Fixed Receiver SAR Images Processed with the Subaperture Range-Doppler Algorithm," in *2006 IEEE International Symposium on Geoscience and Remote Sensing*, 31 July-4 Aug. 2006 2006, pp. 1840-1843, doi: 10.1109/IGARSS.2006.475.
[96] G. Farquharson *et al.*, "The New Capella Space Satellite Generation: Acadia," in *IGARSS 2023 - 2023 IEEE International Geoscience and Remote Sensing Symposium*, 16-21 July 2023 2023, pp. 1513-1516, doi: 10.1109/IGARSS52108.2023.10283030.
[97] W. Junjie *et al.*, "Bi/multi-static Synthetic Aperture Radar Using Spaceborne Illuminator," vol. 12, no. 1, pp. 13-35, 2023, doi: 10.12000/JR22213.
[98] A. K. Gabriel and R. M. Goldstein, "BISTATIC IMAGES FROM SIR-B," in Digest - 1985 International Geoscience and Remote Sensing Symposium (IGARSS '85). Remote Sensing Instrumentation: Technology for Science and Applications., Amherst, MA, USA, 1985: IEEE, in Digest - International Geoscience and Remote Sensing Symposium (IGARSS), p. 112.
[99] K. van't Klooster, "ERS-1, European remote-sensing satellite was launched 20 years ago," in *2011 21st International Crimean Conference" Microwave & Telecommunication Technology"*, 2011: IEEE, pp. 117-118.
[100] H. A. Zebker, T. G. Farr, R. P. Salazar, and T. H. Dixon, "Mapping the world's topography using radar interferometry: the TOPSAT mission," *Proceedings of the IEEE,* vol. 82, no. 12, pp. 1774-1786, 1994, doi: 10.1109/5.338070.
[101] T. Espeter, I. Walterscheid, J. Klare, and J. H. G. Ender, "Synchronization techniques for the bistatic spaceborne/airborne SAR experiment with TerraSAR-X and PAMIR," in *2007 IEEE International Geoscience and Remote Sensing Symposium, IGARSS 2007, June 23, 2007 - June 28, 2007*, Barcelona, Spain, 2007: Institute of Electrical and Electronics Engineers Inc., in International Geoscience and Remote Sensing Symposium (IGARSS), pp. 2160-2163, doi: 10.1109/IGARSS.2007.4423262. [Online]. Available: http://dx.doi.org/10.1109/IGARSS.2007.4423262
[102] T. Espeter *et al.*, "Progress of hybrid bistatic SAR: Synchronization experiments and first imaging results," in *7th European Conference on Synthetic Aperture Radar, EUSAR 2008, June 2, 2008 - June 5, 2008*, Friedrichshafen, Germany, 2008, vol. 1-4: Institute of Electrical and Electronics Engineers Inc., in Proceedings of the European Conference on Synthetic Aperture Radar, EUSAR.
[103] I. Walterscheid, T. Espeter, and J. H. G. Ender, "Performance analysis of a hybrid bistatic SAR system operating in the double sliding spotlight mode," in *2007 IEEE International Geoscience and Remote Sensing Symposium, IGARSS 2007, June 23, 2007 - June 28, 2007*, Barcelona, Spain, 2007: Institute of Electrical and Electronics Engineers Inc., in International Geoscience and Remote Sensing Symposium (IGARSS), pp. 2144-2147, doi: 10.1109/IGARSS.2007.4423258. [Online]. Available: http://dx.doi.org/10.1109/IGARSS.2007.4423258
[104] M. Rodriguez-Cassola *et al.*, "Bistatic spaceborne-airborne experiment TerraSAR-X/F-SAR: data processing and results," in *2008 IEEE International Geoscience and Remote Sensing Symposium - Proceedings, July 6, 2008 - July 11, 2008*, Boston, MA, United states, 2008, vol. 3: Institute of Electrical and Electronics Engineers Inc., in International Geoscience and Remote Sensing Symposium (IGARSS), 1 ed., pp. III451-III454, doi: 10.1109/IGARSS.2008.4779381. [Online]. Available: http://dx.doi.org/10.1109/IGARSS.2008.4779381
[105] S. Duque, P. Lopez-Dekker, J. C. Merlano, J. J. Mallorqui, and A. Broquetas, "Bistatic Interferometry Using Fixed Receiver Configurations," in *7th European Conference on Synthetic Aperture Radar*, 2-5 June 2008 2008, pp. 1-4.
[106] S. Duque, P. Lopez-Dekker, J. J. Mallorqui, and J. C. Merlano, "Back and Forward Bistatic Interferometry," in *IGARSS 2008 - 2008 IEEE International Geoscience and Remote Sensing Symposium*, 7-11 July 2008 2008, vol. 3, pp. III - 601-III - 604, doi: 10.1109/IGARSS.2008.4779419.
[107] S. Duque, P. López-Dekker, J. J. Mallorquí, and J. C. Merlano, "Repeat-pass interferometry using a fixed-receiver and ERS-2/ENVISAT as transmitters of opportunity," in *2009 IEEE International Geoscience and Remote Sensing Symposium*, 12-17 July 2009 2009, vol. 2, pp. II-246-II-249, doi: 10.1109/IGARSS.2009.5418054.
[108] S. Duque, P. López-Dekker, J. C. Merlano, and J. J. Mallorquí, "Bistatic SAR tomography: Processing and experimental results," in *2010 IEEE International Geoscience and Remote Sensing Symposium*, 25-30 July 2010 2010, pp. 154-157, doi: 10.1109/IGARSS.2010.5649760.
[109] H. Nies, F. Behner, S. Reuter, O. Loffeld, and R. Wang, "SAR Experiments in a Bistatic Hybrid Configuration for Generating PolInSAR Data with TerraSAR-X Illumination," in *8th European Conference on Synthetic Aperture Radar*, 7-10 June 2010 2010, pp. 1-4.

[110] F. Behner, S. Reuter, H. Nies, and O. Loffeld, "High resolution bistatic experiments using TerraSAR-X staring spotlight mode and the very high resolution SAR mode of the Fraunhofer FHR PAMIR system," in *Proceedings of EUSAR 2016: 11th European Conference on Synthetic Aperture Radar*, 2016: VDE, pp. 1-4.
[111] F. Behner, S. Reuter, H. Nies, and O. Loffeld, "Synchronization and Processing in the HITCHHIKER Bistatic SAR Experiment," *IEEE Journal of Selected Topics in Applied Earth Observations and Remote Sensing,* vol. 9, no. 3, pp. 1028-1035, 2016, doi: 10.1109/jstars.2015.2471082.
[112] F. Behner, S. Reuter, H. Nies, J. M. C. Muñoz, M. G. Rodriguez, and O. Loffeld, "Characterization of the PAZ X-Band SAR Using the HITCHHIKER Ground Receiver," *IEEE Geoscience and Remote Sensing Letters,* vol. 19, pp. 1-5, 2022, doi: 10.1109/lgrs.2021.3102748.
[113] A. Anghel, R. Cacoveanu, M. Ciuca, B. Rommen, and S. Ciochina, "Multichannel Ground-Based Bistatic SAR Receiver for Single-Pass Opportunistic Tomography," *IEEE Transactions on Geoscience and Remote Sensing,* vol. 61, pp. 1-19, 2023, doi: 10.1109/tgrs.2023.3294124.
[114] A. Anghel, R. Cacoveanu, and M. Datcu, "Phase sensitivity analysis of spaceborne transmitter—Stationary ground-based receiver bistatic SAR interferometry with one imaging channel," in *2017 IEEE International Geoscience and Remote Sensing Symposium (IGARSS)*, 2017: IEEE, pp. 1051-1054, doi: 10.1109/IGARSS.2017.8127136.
[115] A. Anghel, R. Cacoveanu, and M. Datcu, "Repeat-Pass Spaceborne Transmitter-Stationary Receiver Bistatic SAR Interferometry-First Results," in *IGARSS 2018-2018 IEEE International Geoscience and Remote Sensing Symposium*, 2018: IEEE, pp. 3651-3654, doi: 10.1109/IGARSS.2018.8517288.
[116] A. Anghel, R. Cacoveanu, A.-S. Moldovan, C. Savlovschi, B. Rommen, and M. Datcu, "Bistatic SAR imaging with Sentinel-1 operating in TOPSAR mode," in *2017 IEEE Radar Conference (RadarConf)*, 2017: IEEE, pp. 0601-0605, doi: 10.1109/RADAR.2017.7944274.
[117] M. Ciuca, A. Anghel, R. Cacoveanu, B. Rommen, and S. Ciochina, "Single-Pass Spaceborne Transmitter-Stationary Receiver Bistatic SAR Tomography-Novel Solution with 3 Imaging Channels," in *IGARSS 2020-2020 IEEE International Geoscience and Remote Sensing Symposium*, 2020: IEEE, pp. 124-127, doi: 10.1109/IGARSS39084.2020.9323678.
[118] M. Ciuca, A. Anghel, R. Cacoveanu, G. Vasile, M. Gay, and S. Ciochina, "Spaceborne transmitter-stationary receiver bistatic SAR Polarimetry-Experimental Results," in *IGARSS 2020-2020 IEEE International Geoscience and Remote Sensing Symposium*, 2020: IEEE, pp. 3869-3872, doi: 10.1109/IGARSS39084.2020.9324129.
[119] A. Focsa, A. Anghel, and M. Datcu, "A Compressive-Sensing Approach for Opportunistic Bistatic SAR Imaging Enhancement by Harnessing Sparse Multiaperture Data," *IEEE Transactions on Geoscience and Remote Sensing,* vol. 60, pp. 1-14, 2022, doi: 10.1109/tgrs.2021.3071861.
[120] F. Rosu, A. Anghel, R. Cacoveanu, B. Rommen, and M. Datcu, "Multiaperture Focusing for Spaceborne Transmitter/Ground-Based Receiver Bistatic SAR," *IEEE Journal of Selected Topics in Applied Earth Observations and Remote Sensing,* vol. 13, pp. 5823-5832, 2020, doi: 10.1109/jstars.2020.3025058.
[121] D. A. Yocky and D. E. Wahl, "Bistatic SAR: Imagery & Image Products," Sandia National Lab.(SNL-NM), Albuquerque, NM (United States), 2014.
[122] F. Liu, X. Fan, T. Zhang, and Q. Liu, "GNSS-Based SAR Interferometry for 3-D Deformation Retrieval: Algorithms and Feasibility Study," *IEEE Transactions on Geoscience and Remote Sensing,* vol. 56, no. 10, pp. 1-13, 2018, doi: 10.1109/tgrs.2018.2825220.
[123] Z. Wang, F. Liu, R. Lv, and S. Zhang, "Data Acquisition of GNSS-Based InSAR: Joint Accuracy-Efficiency Optimization of 3-D Deformation Retrieval," *IEEE Journal of Selected Topics in Applied Earth Observations and Remote Sensing,* vol. 15, pp. 7886-7898, 2022, doi: 10.1109/jstars.2022.3206110.
[124] T. Zeng, D. Ao, C. Hu, K. Zhang, and T. Zhang, "Multi-angle BiSAR images enhancement and scatting characteristics analysis," in *2014 International Radar Conference*, 13-17 Oct. 2014 2014, pp. 1-5, doi: 10.1109/RADAR.2014.7060418.
[125] T. Zeng, T. Zhang, W. Tian, and C. Hu, "A novel subsidence monitoring technique based on space-surface bistatic differential interferometry using GNSS as transmitters," *Science China Information Sciences,* vol. 58, no. 6, pp. 1-16, 2015, doi: 10.1007/s11432-015-5336-4.
[126] Z. Zeng, M. Antoniou, Q. Zhang, M. Hui, and M. Cherniakov, "Multi-perspective GNSS-based passive BSAR: Preliminary experimental results," in *2013 14th International Radar Symposium (IRS)*, 2013, vol. 1: IEEE, pp. 467-472.
[127] Q. Zhang, W. Chang, Z. Zeng, and Z. Dong, "An integrative synchronization and imaging algorithm for GNSS-based BSAR," *Science China Information Sciences,* vol. 58, no. 6, pp. 1-15, 2015, doi: 10.1007/s11432-015-5319-5.
[128] Z. Sun *et al.*, "A Novel Frequency-Domain Focusing Method for Geosynchronous Low-Earth-Orbit Bistatic SAR in Sliding-Spotlight Mode," *Remote Sensing,* vol. 14, no. 13, p. 3178, 2022, doi: 10.3390/rs14133178.
[129] M. Ciuca, A. Anghel, R. Cacoveanu, B. Rommen, and S. Ciochina, "Single-Pass Spaceborne Transmitter-Stationary Receiver Bistatic SAR Tomography - Novel Solution with 3 Imaging Channels," in *IGARSS 2020 - 2020 IEEE International Geoscience and Remote Sensing Symposium*, 26 Sept.-2 Oct. 2020 2020, pp. 124-127, doi: 10.1109/IGARSS39084.2020.9323678.
[130] Y. Li, Y. Zhang, Z. Chen, and C. Hu, "Noncooperative Repeat-pass Space-Surface Bistatic InSAR: Method and Processing," *IEEE Transactions on Geoscience and Remote Sensing,* vol. 63, 2025, Art no. 5200618.
[131] Z. Chen *et al.*, "Repeat-Pass Space-surface bistatic SAR tomography: accurate imaging and first experiment," *SCIENCE CHINA Information Sciences,* 2024.
[132] K. Sarabandi, J. Kellndorfer, and L. E. Pierce, GLORIA: Geostationary/Low-Earth Orbiting Radar Image Acquisition System: A Multi-Static GEO/LEO Synthetic Aperture Radar Satellite Constellation for Earth Observation. 2003, pp. 773-775 vol.2.
[133] W. Junjie, S. Zhichao, H. Yulin, Y. Jianyu, L. Youxin, and W. Zhimin, "Geosynchronous spaceborne-airborne bistatic SAR: Potentials and prospects," in *2015 IEEE Radar Conference (RadarCon)*, 10-15 May 2015 2015, pp. 1172-1176, doi: 10.1109/RADAR.2015.7131171. [Online]. Available: https://ieeexplore.ieee.org/ielx7/7120813/7130933/07131171.pdf?tp=&arnumber=7131171&isnumber=7130933
[134] J. Wu *et al.*, "Geosynchronous spaceborne-airborne bistatic SAR for earth observation: Advantages and main aspects," in *2016 IEEE 13th International Conference on Signal Processing (ICSP)*, 6-10 Nov. 2016 2016, pp. 91-95, doi: 10.1109/ICSP.2016.7877803. [Online]. Available: https://ieeexplore.ieee.org/ielx7/7870828/7877780/07877803.pdf?tp=&arnumber=7877803&isnumber=7877780
[135] Y. Cheng, S. Zhang, B. Zhao, and C. Hu, "SA-based orbital design method for GEO-BiSAR resolution improvement," in *2017 XXXIInd General Assembly and Scientific Symposium of the International Union of Radio Science (URSI GASS)*, 2017: IEEE, pp. 1-4, doi: 10.23919/URSIGASS.2017.8105222.
[136] H. An, J. Wu, K. C. Teh, Z. Sun, and J. Yang, "Geosynchronous Spaceborne–Airborne Bistatic SAR Imaging Based on Fast Low-Rank and Sparse Matrices Recovery," *IEEE Transactions on Geoscience and Remote Sensing,* vol. 60, pp. 1-14, 2022, doi: 10.1109/tgrs.2021.3081099.
[137] C. Cui, X. Dong, Z. Chen, C. Hu, and W. Tian, "A Long-Time Coherent Integration STAP for GEO Spaceborne-Airborne Bistatic SAR," *Remote Sensing,* vol. 14, no. 3, p. 593, 2022, doi: 10.3390/rs14030593.
[138] G. Guttrich, W. Sievers, and N. Tomljanovich, "Wide area surveillance concepts based on geosynchronous illumination and bistatic unmanned airborne vehicles or satellite reception," in *Proceedings of the 1997 IEEE national radar conference*, 1997: IEEE, pp. 126-131, doi: 10.1109/NRC.1997.588225.
[139] J. Wu, Z. Sun, H. An, J. Qu, and J. Yang, "Azimuth Signal Multichannel Reconstruction and Channel Configuration Design for Geosynchronous Spaceborne–Airborne Bistatic SAR," *IEEE Transactions on Geoscience and Remote Sensing,* vol. 57, no. 4, pp. 1861-1872, 2019, doi: 10.1109/tgrs.2018.2869835.
[140] C. Hu, Z. Chen, Y. Li, X. Dong, and S. Hobbs, "Research progress on geosynchronous synthetic aperture radar," *Fundamental Research,* vol. 1, no. 3, pp. 346-363, 2021, doi: https://doi.org/10.1016/j.fmre.2021.04.008.
[141] "China launches first geosynchronous orbit radar satellite," A. Jones, Ed., ed, 2023, pp. https://spacenews.com/china-launches-first-geosynchronous-orbit-radar-satellite/.
[142] X. Dong, C. Cui, Y. Li, and C. Hu, "Geosynchronous Spaceborne-Airborne Bistatic Moving Target Indication System: Performance Analysis and Configuration Design," *Remote Sensing,* vol. 12, no. 11, p. 1810, 2020, doi: 10.3390/rs12111810.
[143] Z.-h. Zhang, Z. Bao, M.-d. Xing, and J.-y. J. 电. Huang, "The analysis of SNR in passive distributed microsatellites SAR system," vol. 29, no. 1, pp. 15-18, 2007, doi: 10.3724/SP.J.1146.2005.00442.
[144] J. Zheng, M. Ding, L. Sun, and H. Liu, "Distributed Stochastic Algorithm Based on Enhanced Genetic Algorithm for Path Planning of Multi-UAV Cooperative Area Search," *IEEE Transactions on Intelligent*

Transportation Systems, vol. 24, no. 8, pp. 8290-8303, 2023, doi: 10.1109/tits.2023.3258482.
[145] Z. Sun *et al.*, "3-D path planning for GEO-UAV bistatic SAR using multiobjective evolutionary algorithms," in *2016 IEEE Radar Conference (RadarConf)*, 2016: IEEE, pp. 1-5, doi: 10.1109/RADAR.2016.7485189.
[146] Z. Sun, J. Wu, J. Yang, Y. Huang, C. Li, and D. Li, "Path Planning for GEO-UAV Bistatic SAR Using Constrained Adaptive Multiobjective Differential Evolution," *IEEE Transactions on Geoscience and Remote Sensing,* vol. 54, no. 11, pp. 6444-6457, 2016, doi: 10.1109/tgrs.2016.2585184.
[147] Z. Sun, J. Wu, J. Pei, Z. Li, Y. Huang, and J. Yang, "Inclined Geosynchronous Spaceborne–Airborne Bistatic SAR: Performance Analysis and Mission Design," *IEEE Transactions on Geoscience and Remote Sensing,* vol. 54, no. 1, pp. 343-357, 2016, doi: 10.1109/tgrs.2015.2457034.
[148] W.-Q. Wang and H. Shao, "Azimuth-Variant Signal Processing in High-Altitude Platform Passive SAR with Spaceborne/Airborne Transmitter," *Remote Sensing,* vol. 5, no. 3, pp. 1292-1310, 2013, doi: 10.3390/rs5031292.
[149] Z. Liu, Z. Li, C. Dai, H. Huang, and X. Zhang, "Efficient Nonuniform Fourier Reconstruction for Spaceborne/Airborne Bistatic SAR," *IEEE Geoscience and Remote Sensing Letters,* vol. 11, no. 1, pp. 191-195, 2014, doi: 10.1109/lgrs.2013.2252144.
[150] M. Rodriguez-Cassola, P. Prats, G. Krieger, and A. Moreira, "Efficient Time-Domain Image Formation with Precise Topography Accommodation for General Bistatic SAR Configurations," *IEEE Transactions on Aerospace and Electronic Systems,* vol. 47, no. 4, pp. 2949-2966, 2011, doi: 10.1109/taes.2011.6034676.
[151] T. Espeter, I. Walterscheid, J. Klare, and J. H. G. Ender, "Synchronization techniques for the bistatic spaceborne/airborne SAR experiment with TerraSAR-X and PAMIR," in *2007 IEEE International Geoscience and Remote Sensing Symposium*, 2007: IEEE, pp. 2160-2163, doi: 10.1109/IGARSS.2007.4423262.
[152] W.-Q. Wang, C. Ding, X. J. I. R. Liang, Sonar, and Navigation, "Time and phase synchronisation via direct-path signal for bistatic synthetic aperture radar systems," vol. 2, no. 1, pp. 1-11, 2008, doi: 10.1049/iet-rsn：20060097.
[153] Y. Zhang, W. Xiong, X. Dong, and C. Hu, "A Novel Azimuth Spectrum Reconstruction and Imaging Method for Moving Targets in Geosynchronous Spaceborne–Airborne Bistatic Multichannel SAR," *IEEE Transactions on Geoscience and Remote Sensing,* vol. 58, no. 8, pp. 5976-5991, 2020, doi: 10.1109/tgrs.2020.2974531.
[154] W. Xu *et al.*, "Azimuth Multichannel Reconstruction for Moving Targets in Geosynchronous Spaceborne–Airborne Bistatic SAR," *Remote Sensing,* vol. 12, no. 11, p. 1703, 2020, doi: 10.3390/rs12111703.
[155] H. An, J. Wu, K. C. Teh, Z. Sun, and J. Yang, "Simultaneous Moving and Stationary Target Imaging for Geosynchronous Spaceborne-Airborne Bistatic SAR Based on Sparse Separation," *IEEE Transactions on Geoscience and Remote Sensing,* vol. 59, no. 8, pp. 6722-6735, 2021, doi: 10.1109/tgrs.2020.3025802.
[156] C. Cui, X. Dong, Y. Li, Z. Chen, and X. Li, "DNN With Similarity Constraint for GEO SA-BSAR Moving Target Imaging," *IEEE Geoscience and Remote Sensing Letters,* vol. 19, pp. 1-5, 2022, doi: 10.1109/lgrs.2022.3196674.
[157] W. Chenghao, W. Zhanze, L. I. U. Feifeng, H. Cheng, and Z. Tao, "Geometry optimization of bistatic SAR with GNSS transmitters and sloping fields imaging," *JOURNAL OF SIGNAL PROCESSING,* vol. 37, no. 7, pp. 1171-1179, 2021, doi: 10.16798/j.issn.1003-0530.2021.07.006.
[158] L. Cazzani *et al.*, "A ground-based parasitic SAR experiment," *IEEE Transactions on Geoscience and Remote Sensing,* vol. 38, no. 5, pp. 2132-2141, 2000, doi: 10.1109/36.868872.
[159] H. Nies, F. Behner, S. Reuter, and O. Loffeld, "First Results of Passive Radar Imaging and Tracking Using Geostationary Satellites," presented at the 2018 15th European Radar Conference (EuRAD), 2018.
[160] Z. M. Kassas *et al.*, "Navigation with Multi-Constellation LEO Satellite Signals of Opportunity: Starlink, OneWeb, Orbcomm, and Iridium," in *2023 IEEE/ION Position, Location and Navigation Symposium (PLANS)*, 24-27 April 2023 2023, pp. 338-343, doi: 10.1109/PLANS53410.2023.10140066.
[161] S. Kozhaya, H. Kanj, and Z. M. Kassas, "Multi-Constellation Blind Beacon Estimation, Doppler Tracking, and Opportunistic Positioning with OneWeb, Starlink, Iridium NEXT, and Orbcomm LEO Satellites," in *2023 IEEE/ION Position, Location and Navigation Symposium (PLANS)*, 24-27 April 2023 2023, pp. 1184-1195, doi: 10.1109/PLANS53410.2023.10139969.
[162] M. C. Alp Sayin, Michail Antoniou, "Passive radar using Starlink transmissions: A theoretical study," in *20TH INTERNATIONAL RADAR SYMPOSIUM (IRS)*, New York, 2019, doi: 10.23919/IRS.2019.8768105.
[163] P. Gomez-del-Hoyo, P. Samczynski, and F. Michalak, "Analysis of Starlink Users' downlink for passive radar applications: signal characteristics and ambiguity function performance," presented at the 2023 IEEE Radar Conference (RadarConf23), New York, 2023.
[164] K. G. Pedro Gomez-del-Hoyo, Piotr Samczynski, "The STARLINK-based passive radar: preliminary study and first illuminator signal measurements," in *23RD INTERNATIONAL RADAR SYMPOSIUM (IRS)*, New York, 2022, doi: 10.23919/IRS54158.2022.9905046.
[165] R. Blázquez-García, D. Cristallini, M. Ummenhofer, V. Seidel, J. Heckenbach, and D. O'Hagan, "Capabilities and challenges of passive radar systems based on broadband low-Earth orbit communication satellites," *IET Radar, Sonar & Navigation,* vol. 18, no. 1, pp. 78-92, 2023, doi: 10.1049/rsn2.12446.
[166] M. Tian *et al.*, "Multiobjective optimal waveform design for TDS-OFDM integrated radar and communication systems," in *2021 CIE International Conference on Radar (Radar)*, 15-19 Dec. 2021 2021, pp. 2907-2911, doi: 10.1109/Radar53847.2021.10028336.
[167] Y. Liu, G. Liao, J. Xu, Z. Yang, and Y. Zhang, "Adaptive OFDM Integrated Radar and Communications Waveform Design Based on Information Theory," *IEEE Communications Letters,* vol. 21, no. 10, pp. 2174-2177, 2017, doi: 10.1109/lcomm.2017.2723890.
[168] M. Antoniou, M. Cherniakov, R. Saini, J. Edwards, and R. Zuo, "Modified Range-Doppler Algorithm for Space-Surface BSAR imaging," in *2006 CIE International Conference on Radar*, 16-19 Oct. 2006 2006, pp. 1-4, doi: 10.1109/ICR.2006.343429.
[169] Z. Wang, F. Liu, Z. Xu, and J. Zhou, "High-Coherence Oriented Image Formation Algorithm Based on Adaptive Elevation Ramp Fitting for GNSS-Based InBSAR Systems," *IEEE Transactions on Geoscience and Remote Sensing,* vol. 62, pp. 1-14, 2024, doi: 10.1109/tgrs.2024.3388465.
[170] F. Liu, R. Lv, Z. Wang, Z. Xu, and C. Wang, "An Adaptive Fake Permanent Scatterer Removal Algorithm Based on Direct Signal Reconstruction of Multiparameter Estimation for GNSS-InBSAR," *IEEE Geoscience and Remote Sensing Letters,* vol. 21, pp. 1-5, 2024, doi: 10.1109/lgrs.2024.3368523.
[171] Z. Wang, F. Liu, R. Shang, and J. Zhou, "A Novel Multiangle Images Association Algorithm Based on Supervised Areas for GNSS-Based InSAR," *IEEE Geoscience and Remote Sensing Letters,* vol. 20, pp. 1-5, 2023, doi: 10.1109/lgrs.2023.3238505.
[172] Z. Wang, F. Liu, T. Zeng, and C. Wang, "Interferometric Phase Error Analysis and Compensation in GNSS-InSAR: A Case Study of Structural Monitoring," *Remote Sensing,* vol. 13, no. 15, 2021, doi: 10.3390/rs13153041.
[173] F. Liu, X. Fan, T. Zhang, and Q. Liu, "GNSS-Based SAR Interferometry for 3-D Deformation Retrieval: Algorithms and Feasibility Study," *IEEE Transactions on Geoence and Remote Sensing,* vol. 56, no. 99, pp. 5736-5748, 2018.
[174] D. Yunkai, z. yongwei, Z. zhimin, W. Wei, and Z. Heng, "Orthogonal Waveform Design with Fractional Programming on the Ambiguity Suppression of SAR System," *SCIENCE CHINA Information Sciences,* 2024, doi: https://doi.org/10.1007/s11432-023-4076-7.
[175] H. BI, Y. SONG, Y. YIN, J. ZHANG, W. HONG, and Y. WU, "A novel sparse SAR unambiguous imaging method based on mixed-norm optimization," *SCIENCE CHINA Information Sciences,* vol. 66, no. 11, p. 219302, 2023, doi: https://doi.org/10.1007/s11432-022-3814-8.
[176] T. Kraus, G. Krieger, M. Bachmann, and A. Moreira, "Spaceborne Demonstration of Distributed SAR Imaging With TerraSAR-X and TanDEM-X," *IEEE Geoscience and Remote Sensing Letters,* vol. 16, no. 11, pp. 1731-1735, 2019, doi: 10.1109/lgrs.2019.2907371.
[177] T. Zeng, T. Zhang, W. Tian, and C. Hu, "Space-Surface Bistatic SAR Image Enhancement Based on Repeat-Pass Coherent Fusion With Beidou-2/Compass-2 as Illuminators," *IEEE Geoscience and Remote Sensing Letters,* vol. 13, no. 12, pp. 1832-1836, 2016, doi: 10.1109/lgrs.2016.2614337.
[178] M. Hui, M. Antoniou, and M. Cherniakov, "Passive GNSS-Based SAR Resolution Improvement Using Joint Galileo E5 Signals," *IEEE Geoscience and Remote Sensing Letters,* vol. 12, no. 8, pp. 1640-1644, 2015, doi: 10.1109/lgrs.2015.2417594.
[179] X. Chen, Z. Chen, Y. Li, C. Hu, X. Dong, and S. Hobbs, "Improving 2-D Resolution in Geosynchronous SAR via Spatial Spectrum Synthesis: Method and Verification," *IEEE Journal of Selected Topics in Applied Earth Observations and Remote Sensing,* vol. 17, pp. 5847-5863, 2024, doi: 10.1109/jstars.2024.3361165.
[180] C. Hu, Z. Chen, X. Dong, and C. Cui, "Multistatic Geosynchronous SAR Resolution Analysis and Grating Lobe Suppression Based on Array Spatial Ambiguity Function," *IEEE Transactions on Geoscience and Remote Sensing,* vol. 58, no. 9, pp. 6020-6038, 2020, doi: 10.1109/tgrs.2020.2969573.
[181] J. Ding, L. Wen, C. Zhong, and O. Loffeld, "Video SAR Moving Target Indication Using Deep Neural Network," *IEEE Transactions on*

Geoscience and Remote Sensing, vol. 58, no. 10, pp. 7194-7204, 2020, doi: 10.1109/tgrs.2020.2980419.
[182] K. Mattingly and S. De, "Computer Vision Techniques Applied to Capella Space VHR X-Band Synthetic Aperture Radar (SAR) Satellite Data to Track Movement: Use Cases Of Glacial Ice and Ships," in *IGARSS 2023 - 2023 IEEE International Geoscience and Remote Sensing Symposium*, 16-21 July 2023 2023, pp. 195-198, doi: 10.1109/IGARSS52108.2023.10281583.
[183] A. Renga, M. D. Graziano, and A. Moccia, "Formation Flying SAR: Analysis of Imaging Performance by Array Theory," *IEEE Transactions on Aerospace and Electronic Systems,* vol. 57, no. 3, pp. 1480-1497, 2021, doi: 10.1109/taes.2020.3043526.
[184] X. Zhao, Y. Li, Z. Chen, Y. Xie, and C. Hu, "A Deep Learning Coregistration Approach for Distributed Geosynchronous SAR Three-Dimensional Deformation Retrieval," in *IGARSS 2023 - 2023 IEEE International Geoscience and Remote Sensing Symposium*, 16-21 July 2023 2023, pp. 1791-1794, doi: 10.1109/IGARSS52108.2023.10283370.
[185] P. Rizzoli *et al.*, "Generation and performance assessment of the global TanDEM-X digital elevation model," *ISPRS Journal of Photogrammetry and Remote Sensing,* vol. 132, pp. 119-139, 2017, doi: 10.1016/j.isprsjprs.2017.08.008.
[186] M. Lachaise, C. González, P. Rizzoli, B. Schweißhelm, and M. Zink, "The New Tandem-X DEM Change Maps Product," in *IGARSS 2022 - 2022 IEEE International Geoscience and Remote Sensing Symposium*, 17-22 July 2022 2022, pp. 5432-5435, doi: 10.1109/IGARSS46834.2022.9883612.
[187] B. Schweisshelm and M. Lachaise, "Tandem-X Dem Change Maps Stacks: Towards Tandem-X 4D," in *IGARSS 2023-2023 IEEE International Geoscience and Remote Sensing Symposium*, 2023: IEEE, pp. 1329-1332, doi: 10.1109/IGARSS52108.2023.10282397.
[188] R. Deo, C. Rossi, M. Eineder, T. Fritz, Y. S. Rao, and M. Lachaise, "Fusion of ascending and descending pass raw TanDEM-X DEM," in *2014 IEEE Geoscience and Remote Sensing Symposium*, 13-18 July 2014 2014, pp. 21-24, doi: 10.1109/IGARSS.2014.6946345.
[189] Y. Luo, Y. Deng, W. Xiang, H. Zhang, C. Yang, and L. Wang, "Radargrammetric 3D Imaging through Composite Registration Method Using Multi-Aspect Synthetic Aperture Radar Imagery," *Remote Sensing,* vol. 16, no. 3, p. 523, 2024, doi: 10.3390/rs16030523.
[190] R. Palama *et al.*, "Radargrammetry DEM Generation Using High-Resolution SAR Imagery Over La Palma During the 2021 Cumbre Vieja Volcanic Eruption," *IEEE Geoscience and Remote Sensing Letters,* vol. 20, pp. 1-5, 2023, doi: 10.1109/lgrs.2023.3238182.
[191] M. Zhu, C. Hu, T. Zeng, Y. Li, and Y. Gao, "Fixed-receiver bistatic interferometric algorithms analysis and implementation," in *2013 IEEE Radar Conference (RadarCon13)*, 29 April-3 May 2013 2013, pp. 1-4, doi: 10.1109/RADAR.2013.6586019.
[192] R. Wang *et al.*, "Double-Channel Bistatic SAR System With Spaceborne Illuminator for 2-D and 3-D SAR Remote Sensing," *IEEE Transactions on Geoscience and Remote Sensing,* vol. 51, no. 8, pp. 4496-4507, 2013, doi: 10.1109/tgrs.2013.2252908.
[193] Y. Zhang, K. Lin, Y. Li, C. Hu, and Z. Chen, "Potential of Topographic Measurement by Time-Series Loose Distributed SAR Interferometry," in *2022 3rd China International SAR Symposium (CISS)*, 2022: IEEE, pp. 1-4, doi: 10.1109/CISS57580.2022.9971257.
[194] M. Nannini *et al.*, "Coherence-based SAR tomography for spaceborne applications," *Remote Sensing of Environment,* vol. 225, pp. 107-114, 2019, doi: 10.1016/j.rse.2019.01.040.
[195] Y. Shi, R. Bamler, Y. Wang, and X. X. Zhu, "SAR Tomography at the Limit: Building Height Reconstruction Using Only 3–5 TanDEM-X Bistatic Interferograms," *IEEE Transactions on Geoscience and Remote Sensing,* vol. 58, no. 11, pp. 8026-8037, 2020, doi: 10.1109/tgrs.2020.2986052.
[196] D. HAN, Z. JIAO, L. ZHOU, C. DING, and Y. WU, "Geometric constraints based 3D reconstruction method of tomographic SAR for buildings," *SCIENCE CHINA Information Sciences,* vol. 66, no. 1, p. 112301, 2023, doi: https://doi.org/10.1007/s11432-022-3521-0.
[197] M. Pardini, A. Torano-Caicoya, F. Kugler, and K. Papathanassiou, "Estimating and understanding vertical structure of forests from multibaseline TanDEM-X Pol-InSAR data," in *2013 IEEE International Geoscience and Remote Sensing Symposium-IGARSS*, 2013: IEEE, pp. 4344-4347, doi: 10.1109/IGARSS.2013.6723796.
[198] O. Frey and E. Meier, "3-D Time-Domain SAR Imaging of a Forest Using Airborne Multibaseline Data at L- and P-Bands," *IEEE Transactions on Geoscience and Remote Sensing,* vol. 49, no. 10, pp. 3660-3664, 2011, doi: 10.1109/TGRS.2011.2128875.
[199] D. Ao, Y. Li, C. Hu, and W. Tian, "Accurate Analysis of Target Characteristic in Bistatic SAR Images: A Dihedral Corner Reflectors Case," *Sensors,* vol. 18, no. 1, 2017, doi: 10.3390/s18010024.
[200] P. Prats-Iraola, P. Lopez-Dekker, F. De Zan, N. Yague-Martinez, M. Zonno, and M. Rodriguez-Cassola, "Performance of 3-D Surface Deformation Estimation for Simultaneous Squinted SAR Acquisitions," *IEEE Transactions on Geoscience and Remote Sensing,* vol. 56, no. 4, pp. 2147-2158, 2018, doi: 10.1109/tgrs.2017.2776140.
[201] Y. Li, P. L. Dekker, and P. Prats-Iraola, "A Multichannel Wiener Filter Method of Deformation Measurement for Simultaneous Multiangle Spaceborne D-InSAR," *IEEE Transactions on Geoscience and Remote Sensing,* vol. 61, pp. 1-15, 2023, doi: 10.1109/tgrs.2023.3330482.
[202] C. Hu, Y. Tian, X. Dong, R. Wang, and T. Long, "Computerized ionospheric tomography based on geosynchronous SAR," *Journal of Geophysical Research: Space Physics,* vol. 122, no. 2, pp. 2686-2705, 2017, doi: 10.1002/2016ja023542.
[203] Y. Li, P. L. Dekker, G. Mulder, L. Iannini, and P. Prats-Iraola, "Differential Tropospheric Delay Estimation by Simultaneous Multi-Angle Repeat-Pass InSAR," *IEEE Transactions on Geoscience and Remote Sensing,* vol. 60, pp. 1-18, 2022, doi: 10.1109/tgrs.2021.3105007.
[204] Y. Li, C. Liu, Z. Chen, and C. Hu, "Differential Tropospheric Tomography using Spaceborne Simultaneous Multi-angle D-InSAR: Method, Optimization, and Performance Analysis," *IEEE Transactions on Geoscience Remote Sensing,* vol. 62, 2024, Art no. 5226714.
[205] M. Kleinherenbrink *et al.*, "Estimating instantaneous sea-ice dynamics from space using the bi-static radar measurements of Earth Explorer 10 candidate Harmony," *The Cryosphere,* vol. 15, no. 7, pp. 3101-3118, 07/06 2021, doi: 10.5194/tc-15-3101-2021.
[206] N. Caldarella *et al.*, "Retrieval of Wind and Total Surface Current Vectors Using Experimental Bidirectional Along-Track Interferometric TanDEM-X Data," *IEEE Transactions on Geoscience and Remote Sensing,* vol. 60, pp. 1-12, 2022, doi: 10.1109/tgrs.2022.3147490.
[207] M. Kleinherenbrink, P. Lopez Dekker, F. Nouguier, and B. Chapron, *Bistatic SAR mapping of ocean-wave spectra*. 2023.
[208] P. López-Dekker, H. Rott, P. Prats-Iraola, B. Chapron, K. Scipal, and E. D. Witte, "Harmony: an Earth Explorer 10 Mission Candidate to Observe Land, Ice, and Ocean Surface Dynamics," in *IGARSS 2019 - 2019 IEEE International Geoscience and Remote Sensing Symposium*, 28 July-2 Aug. 2019 2019, pp. 8381-8384, doi: 10.1109/IGARSS.2019.8897983.
[209] L. Y. Fu Jiayu, Chen Zhiyang, Hu Cheng. "A New Distributed ATI SAR System: GEO-LEO SAR ATI Concept." European Space Agency. https://eo4society.esa.int/training_uploads/seasar2023/SaSAR23Theme8_FutureMissions-compendium-v2.0.pdf (accessed 2023).
[210] D. Sun, Y. Wang, Z. Xu, and Y. Zhang, "Ocean Wave Inversion Using TerraSAR-X and TanDEM-X Images," in *2021 13th International Symposium on Antennas, Propagation and EM Theory (ISAPE)*, 1-4 Dec. 2021 2021, vol. Volume1, pp. 01-03, doi: 10.1109/ISAPE54070.2021.9753368.
[211] D. O. Dammann *et al.*, "New Possibilities Using TS-X and TD-X in Support of Sea Ice Use," in *EUSAR 2018; 12th European Conference on Synthetic Aperture Radar*, 4-7 June 2018 2018, pp. 1-6.

https://dspace.org/

Distributed Spaceborne SAR: a review of systems, applications, and the road ahead

Hu, Cheng; Li, Yuanhao; Chen, Zhiyang; Liu, Feifeng; Zhang, Qingjun ...

2025-06
Institute of Electrical and Electronics Engineers (IEEE)
https://doi.org/10.1109/mgrs.2025.3535412
Hu C, Li Y, Chen Z, et al., (2025) Distributed Spaceborne SAR: A review of systems, applications, and the road ahead. IEEE Geoscience and Remote Sensing Magazine, Volume 13, Issue 2, June 2025, pp. 329-361

Downloaded from a DSpace repository. https://dspace.org/